Radial Line Slot array antennas with scannable beam using impedance surfaces

Elsa Brischoux

Supervisor: Alejandro Valero Nogueira

Co-supervisor: José Ignacio Herranz Herruzo

Abstract

During the last few years, satellite communications have advanced hugely in terms of telecommunications and information transmission. This, apart from a notorious spread of satellite fleets by big organizations in the sector, brings with it a need to continue researching about devices used in these communications. In this work, our intention is to delve into an indispensable device in every satellite communication, antennas. The research has been focused on the scopes of manufacturing and commerce of terrestrial antennas. The memory of this project will focus on Low Profile antennas, which consist of groups of slots in a radial waveguide. In this case, a metasurface will replace the dielectric element, so that losses will be reduced, and an alternative will be used instead of the usual dielectrics. Furthermore, different implementations will be studied in order to be able to recreate a beam steering on the radiation pattern.

Keywords: Satellite communications, Low Profile antennas, Slot arrays, Radial waveguide, Metasurface, Dielectric, Beam-steering.

Resumen

Durante los últimos años, las comunicaciones por satélite han supuesto un gran avance en el ámbito de las telecomunicaciones y de la transmisión de la información. Esto, además de un notorio despliegue de flotas de satélites por parte de grandes entidades dedicadas al sector, trae consigo una necesidad de seguir investigando acerca de los dispositivos empleados en estas comunicaciones. En este trabajo, se pretende profundizar sobre un dispositivo indispensable en toda comunicación por satélite, las antenas. Cuya investigación se ha centrado en ámbitos de fabricación y comerciales de antenas terrestres. La memoria de este trabajo se centrará en antenas de bajo perfil, concretamente en agrupaciones de ranuras en guía de onda radial. En este caso, a modo de elemento dieléctrico, se utiliza una metasuperficie. De esta forma se consigue reducir las pérdidas y representa una alternativa frente a los usuales dieléctricos. Además, se estudiará la implementación necesaria para conseguir desapuntamiento en el diagrama de radiación.

Palabras clave: Comunicaciones por satélite, Antenas de bajo perfil, Agrupaciones de ranuras, Guía de onda radial, Metasuperficie, Dieléctricos, Desapuntamiento.

Resum

Durant el últims anys, les comunicacions per satèl·lit han suposat un gran avanç en l'àmbit de les telecomunicacions i de la tranmisió de la informació. Això, a més d'un notori desplegament de flotes satel·litals per part de grans entitats dedicades al sector, porta amb si una necessitat de continuar investigant sobre els dispositius emprats en aquestes comunicacions. En aquest treball, es pretén aprofundir sobre un dispositiu indispensable en tota comunicació satel·lital, les antenes. La investigació ha estat centrada en àmbits de fabricació i comercials d'antenes terrestres. La memòria d'aquest treball es centrará en antenes de tipus Low Profile, les quals radiquen en agrupacions de ranures en guia d'ona radial. En aques cas, com a element dielèctric s'ha utilitzat una metasuperficie, d'aquesta forma s'aconsegueix reduïr les pèrdues i una alternativa enfront dels usuals dielèctrics d'antena. A més, s'estudiarà la implementació necessaria per aconseguir desapuntament en el diagrama de radiació.

Paraules clau: Comunicacions per satèl·lit, Low profile, Agrupacions de ranures, Guía d'ona radial, Dielèctric, Metasuperficie, Desapuntament.

Contents

List of Figures

List of Tables

Chapter 1

Introduction

This document introduces the research and work carried out for the Bachelor's Degree Final Project of "Bachelor's Degree in Telecommunication Technologies and Services Engineering", entitled "Radial Line Slot array antennas with scannable beam using impedance surfaces". Throughout this document, the process executed to study the metasurface for an RLSA (Radial-Line Slot-Array) antenna will be detailed.

In this first chapter, emphasis will be placed on the motivation that led to the study of this work and the objectives that were taken into consideration. Furthermore, the methodology considered will be discussed and finally a presentation of the structure will be detailed for a better comprehension.

1.1   Motivation

Nowadays, it is well known that telecommunications sector is booming due to the improvements and growth of its technology. An example of such are satellite communications, which apart from coming to prominence during the recent years, are expected to provide revolutionary applications at long term. This increase in the number of satellite communication services has led to the need to use higher frequency bands such as the Ku and Ka bands to make way for new applications.

On the other hand, the fact of using higher frequency values leads to greater transmission bandwidths. This is due to the fact that an average user needs higher transmission speed over time. Thus, the idea of using higher frequencies and, therefore, greater bandwidths, allows us to use smaller devices which results in a decongestion of the electromagnetic spectrum.

However, spectrum has become difficult to manage over the years due to high demand from users and entities that ask for better spectrum management and distribution, while the emergence of new terrestrial technologies such as cellular communications or streaming, limits the exploitation and distribution of the spectrum. Taking this into account, one way to ensure that the spectrum does not congest would be using antennas in higher frequency bands. That is why there is a need to research and develop devices capable of working at these frequencies.

As a result, in this work the study of a type of RLSA antenna in the Ka band is proposed, in such a way that the own data transmission needs are satisfied in those cases in which a low-profile, high gain and efficiency antenna is required. An investigation will be carried out, as well as the implementation of several improvements such as the elimination of the dielectric and its replacement by

a metasurface. The study of the behavior of the antenna and the propagation of the electromagnetic field within the radial waveguide will be presented in the following sections. The antenna will acquire higher efficiency values at high frequency bands as a result of eliminating dielectric losses. In addition, the antenna will have the ability to scan its beam and rotate it so that a link can be established with satellites that are not in a fully vertical position with respect to it.

1.2   Antennas for satellite communication

Satellite communication terminals are hugely advantageous nowadays since they are capable of operating in regions with not far advanced infrastructures. Great number of terminals in terms of SATCOM (Satellite Communications) SOTM (Satellite On The Move) services have already been implemented by many companies. In order to get high speed transmission, Shannon fundamentals [1] must be fulfilled for channels with additive white gaussian noise AWGN [2]. Therefore, to accomplish those statements, EIRP ($P_t \cdot G_t$) value must be high in transmission and figure of merit should provide an accurate value in reception (G_r/T), where P_t is the transmission power, G_t and G_r are the transmission and reception gain and T is the equivalent noise temperature in reception. The frequency work of the antenna considered in this project will be 30 GHz, which is contained in the Ka band (26.5 - 40 GHz). Ka band is considered to be one the most advantageous and used in satellite communications along with the Ku band (12 - 18 GHz). Currently, satellites working at Ka and Ku band are more usual than L (1 - 2 GHz) and S band (2 - 4 GHz) [3].

As mentioned in a previous section, antennas are key elements in terminals and ought to have the following characteristics: narrow beam, low sidelobes, low profile, small weight and size, low power consuming, high reliability, and reasonable price. Three different types can be mentioned: antennas with two-dimensional mechanical scanning, that is reflector antennas and passive arrays. Alternatively, there are antennas with two-dimensional electrical scanning, containing phased arrays. Additionally, antennas with combined scanning can also be found. In those systems the mechanical scanning is situated in the azimuth plane, meanwhile the electrical scanning takes place in the elevation plane. An example of such would be low-profile phased arrays on rotatory platforms.

In the following subsections, several types of antennas for satellite communication will be introduced following the characteristics described in [4] where a study of antennas for SATCOM SOTM is carried out.

1.2.1   Reflector antennas

Reflector antennas provide high gain and reasonable side lobe level. A significant advantage is the capacity to unify transmission and receiving antennas whereas operating in multiple bands. Moreover, this type of antenna is hugely popular in SATCOM because of the fact that high gain and acceptable secondary lobe level can be reached with minimum cost.
Although, the size and high profile of these types of antennas entail some disadvantages. An example of such is shown in Fig. 1.1.
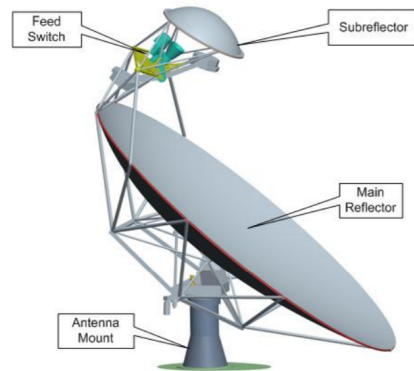
Figure 1.1: Reflector antenna in [5]

1.2.2 Phased array antennas

Antenna arrays consist of a group of several antennas, which are normally dipoles, working as a single antenna. Some of them present different implementations, one example of that could be a type of array which consists of two types of scanning, one in the azimuth plane executed by mechanical rotation of the antenna itself, and the other in the elevation plane. An example of such consisting of a low-profile array for Ku-band was implemented by Intelwaves Technology Ltd. Meanwhile, production of this type of antenna is mainly realized by ThinSat company.

Figure 1.2: Phased array antenna in [6]

Another example of such in [4] are phased array antennas implemented by Phasor company as shown in Fig. 1.3. Phasor antennas are able to dynamically control amplitude and phase level for each element of the structure. Therefore, that allows to electronically orient the beam in an efficient way.
Some of the advantages are:

- Low dimensions.

- Several antennas can be used to form a unique logic antenna.

- Capacity of having multiple beams in order to point at two different satellite at a time.

- Beam shape can be modified, including the possibility of forcing nulls to avoid interferences among satellites.

- No mobile parts are needed to form the beam.
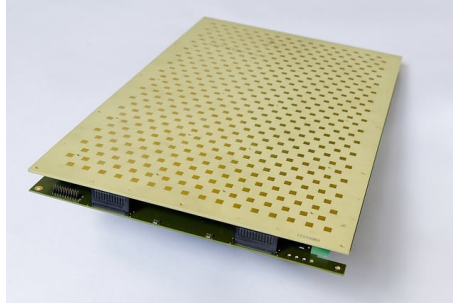
Figure 1.3: Phased array implemented by Phasor company in [4]

1.3   Beam-Steering Lens Antennas for Ku-band applications

Nowadays, there is a massive interest in finding low dimension and weight antennas at a reasonable price for satellite communication on the move (SOTM). The most difficult part is to find a way to combine those requirements along with high gain and beem-steering capacity. An example of a beem-steering method will be discussed in this section based on the Risley prism theory [7].

The arrangement of a beam-steerable antenna is based on 3 lenses as shown in Fig. 1.4: stationary lens 0, rotatable lens 1 and 2. Altogether, the lenses can effectuate a 360º transmission phase range by means of the rotation of multiple elliptical hole components the lenses are composed of. Metasurface and lens 0 radiate a circularly polarized plane wave. The incident wave on lens 1 makes the beam converge and deflect in several directions. Thus, the beam is deflected another time when it reaches lens 2 causing lens 1 and lens 2 to rotate round the antenna axis.
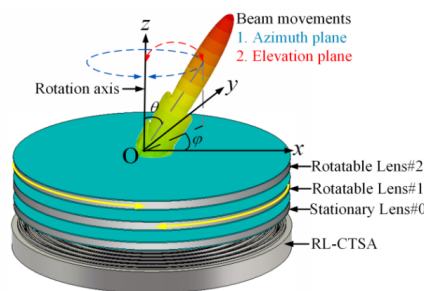
Figure 1.4: Risley prism theory in [7]

In this project, the mechanics behind the RLSA functioning can also be related to the Risley prism theory. But, in this case the patches which form the metasurface and the distance among them altogether with slots distribution is what makes the beam rotate and effectuate a 360º transmission phase range. So, the similarity with the Risley theory comes when the platform containing the slots is rotated and is, indeed, able to duplicate the tilt value. The main advantage comparing to Risley principal, is the simplicity of just rotating a unique platform instead of two, in order to get higher tilt values.

1.4 Objectives

This project consists of designing a beam steering RLSA antenna at Ka-band, the center frequency of which will be 30 GHz. The dielectric used in the RLSA to provide the slow wave propagation within the parallel-plate waveguide will be replaced by a metasurface. In the first place, a study of such metasurface will be needed. Then, some further studies will be carried out in order to find the most efficient procedure to develop the beam-steering comparing to the broadside direction. Finally, the beam will be rotated in order to reach higher tilt values.

1.5 Methodology

The tasks taken into consideration to achieve the objectives of the project are detailed as follows:

1. A detailed explanation of the theory of the antenna considered during this project and steps followed to implement it.

2. Study of the metasurface formed by a periodic structure equivalent to a relative permittivity value.

3. Simulation of the antenna without considering the slots on the upper plate to verify that the electric field propagates properly.

4. Simulation of the antenna considering the slots in order analyze the beam-steering value obtained.

5. Rotation of the upper plate containing the slots.

6. Analysis of the final results.

Two simulation and analysis software suites are considered during this project:

- CST Microwave Studio: The simulations of the antenna were carried out using this program. The electric field and radiation patterns were analyzed as it is an electromagnetic simulation software [8].

- Matlab: Numerical computation program [9]. This program has been used in order to implement the structure of the metasurface, generation of slots and analysis of the radiation patterns.

1.6 Structure of the project

This structure represents the steps followed during the study:

- Designs and description of an RLSA antenna (Chapter 2).

- Design and analysis of a metasurface in order to replace an homogeneous dielectric (Chapter 3).

- Study of different metasurface structures (Chapter 3).

- Simulation and study of beam-steering values of the antenna (Chapter 4).

- Study of the result of rotating the upper plate of the waveguide (Chapter 4).

- Conclusions (Chapter 5).

Chapter 2

CP-RLSA: Circularly Polarized RLSA

In this chapter, the following points will be discussed: description of RLSA antennas and some examples, antenna topology and general design considerations. Furthermore, design and analysis codes have already been provided in [10], so the best parameters for the structure to work properly have been chosen.

2.1   RLSA description

Radial Line Slot Antennas (RLSA) belong to a type of waveguide antenna whose design consists of two surfaces where the upper surface includes a radiation slots distribution, whereas the other contains a feeder element at the center of it.

As specified in [11], at the upper surface around the feed probe, there is a section free of slots in order to allow waves to settle inside the radial waveguide. The position and orientation of the slots will lead out to different kinds of wave polarizations which can be either transmitted or received. Moreover, RLSAs include some features such as high gain and high efficiency as well as the aptness of mass production and low weight, which together imply more advantages with regard to parabolic antennas. Those antennas are made for diverse frequency applications including Wi-Fi, 5G, etc.

On the first place, a previous version linearly polarized was proposed for radar applications [12]. Later, in 1985 a circularly polarized RLSA was suggested at the Tokyo Institute of Technology, with a gain of 36.3 dBi, 60 cm of diameter and working at the frequency of 12 GHz [13]. As mentioned above, the antenna presents a double layer inner structure, two surfaces, one of them has slots over it, the other has the feeder without slots. In that layer TEM mode waves are generated and propagate outwards along the radial direction until a 180º bend is found. The wave is reflected to the upper layer where while propagating toward the center of the structure, the slots get excited. Nevertheless, due to the difficulties as regards design and optimization matters as well as implementing the bend, a new structure was considered in [14], a single-layer CP-RLSA (SL-RLSA). This model consists of a radial guide fed by a homogenous dielectric in the center.
In this type of antennas, the progressive wave propagation itself causes the slots excitement, and because of that an inner dielectric is needed for the slots to be in phase, and diffraction lobes not

to appear.

Linearly-polarized RLSA antennas are not as popular as CP-RLSA, partly because of the position of the slots which can cause unwanted reflections. For that reason, the model of a CP-RLSA antenna will be used in this work. Moreover, in satellite communications circular polarization is used in the working band.
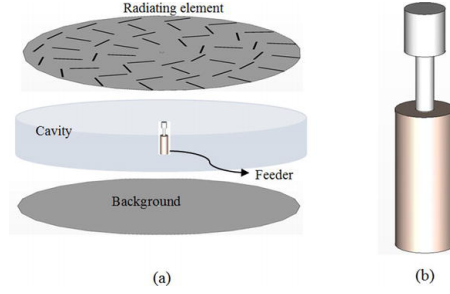
Figure 2.1: RLSA antenna description in [11]

2.2 Design and slots generation

This section describes the process followed in [10] to generate the slots distribution. As mentioned previously the antenna will work at 30 GHz. It will be mainly composed of a radial guide, which consists of parallel plate guide, excited by a coaxial probe in the center. According to waveguide theory and due to the type of feeding and geometry of the guide, a cylindrical TEM mode would propagate whenever $h < \lambda_g/2$, where λ_g is the wavelength inside the guide and can be calculated as follows $\lambda_g = \lambda_o/\sqrt{\epsilon_r}$, where λ_o is the vacuum wavelength and ϵ_r is the dielectric relative permittivity. This mode propagates outwards in a radial direction from the position of the probe. This way, the power transported by the field is coupled to the slots, progressively radiating until it reaches the end of the waveguide. The termination of the guide can be done, up to a point, with an adapted load that absorbs the residual power. However, in practical designs, it is typical to use a final shortcircuit in order to minimize losses.

As mentioned previously, in the case of a CP-RLSA antenna which will be considered in this work due to its great performance, the radiator component is composed of a pair of slots separated a distance of $\lambda_g/4$ from each other in order to generate a difference of phase which will excite them in quadrature. Returning to the case of CP-RLSA, circular polarization is achieved by placing the slots in such a way their orientation is defined by angles of $\theta_1 = \pi/4$ and $\theta_2 = 3\pi/4$, with respect to the radial axis. The Fig. 2.2 shows the representation of the slots in more detail, as well as the representation of a single-layer CP-RLSA. This basic radiating unit is grouped by repeating itself along a spiral whose direction of rotation is counterclockwise direction, centered at the origin of coordinates. In such a way that a coherent sum of circular radiation to the right is achieved, as long as the existing spacing between two turns of the mentioned spiral is equal to the wavelength inside the waveguide, that is, $S_\rho = \lambda_g$. In order to prevent the appearance of diffraction lobes, using a material such as air must be avoided. In this way, a dielectric would be introduced whose relative permittivity ought to be greater than one.

(a) CP-RLSA antenna   **(b) Detailed slots distribution**
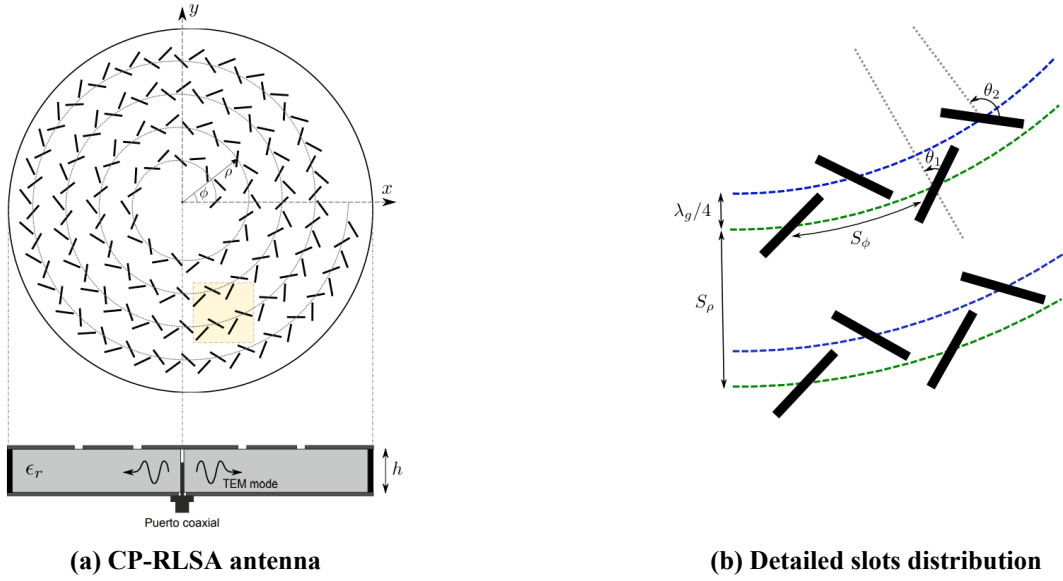
Figure 2.2: CP-RLSA antenna and its slots distribution

Regarding the existing spacing between consecutive slots, the uniformity of the fields in the aperture shows improvements when the slots are closer to each other, in such a way that and optimal case would be achieved when the slots are overlapping. Finally, the distance between the first slot and the feeder will still be unknown, that is ρ_0. This distance will be defined as $\rho_0 = \lambda_g$ so that, optimal waveguide dimensions will be reached.

Considering the characteristics specified above, the slots could already be unfolded and located in a spiral of N turns. However, in order to maintain a uniform excitation for each pair of slots, it is necessary to adjust the length of the slots in such a way as to compensate the dropping of the cylindrical mode in the radial direction. This amplitude drop comes from the following relation $\frac{1}{\sqrt{\rho}}$ which comes from the ratio of the TEM mode amplitude. Furthermore, the slots which have already been excited before or, in other words, have previously radiated, must be considered in order to guarantee that the slots are uniformly excited. A solution to this problem lies in a compensation model by means of which a residual power will be established which will denote the desired radiated power and in turn will determine the radiation efficiency value for each of the turns of the spiral. The residual power is defined as $t_{res} = W^{out}/W^{in}$.

Regarding the efficiency values, these should be translated into slot length values. Knowing the value of the radiated power in each pair of slots W^{rad}, the distance from the slots to the feeder ρ_0, the angular spacing between pairs of slots S_ϕ, and the input power W^{in}, the relationship between efficiency and length of the grooves will be obtained. Although, it is an approximate result which will be adjusted and corrected by analyzing the results.

$$\eta = \frac{2\pi\rho_0}{S_\phi} \frac{W^{rad}}{W^{in}} \tag{2.1}$$

After having determined the method that will be used to find the length of the slots, the degrees of freedom suggested by the codes used to generate the CP-RLSA at a central frequency of $f_0 = 30$

GHz must be set. Firstly, the height of the waveguide, h, must be set. This value must be chosen complying with the single-mode propagation criterion, that is $h < \lambda_g/2$ in this way, the cutoff frequency of the second mode is higher than the central one. In [10] the existence of a compromise between illumination and radiation efficiency is verified and demonstrated. Furthermore, when the residual power is low or non-existent, the radiation will be maximum, while the illumination efficiency will be low. This is due to the existence of couplings between slots that will entail low illumination uniformity in the slots aperture.

2.3 CP-RLSA modelling and simulation using CST

In Fig. 2.3, a representation of the slots in CST can be observed once they have been exported (Fig. 2.3a) and after including them in the upper plate (Fig. 2.3b). After this, both plates that form the waveguide are modeled in z- and z +. Then, the dielectric, or else the patch distribution, is added obtaining a structure such as Fig. 2.3. Finally, a discrete port is created and located at the origin of coordinates of the XY plane at a central height inside the waveguide. The upper plate is located 1 mm from the origin, therefore the port will be placed between z = 0.33 mm and z = 0.66 mm. Finally, the antenna boundary conditions are defined. Absorption conditions are established on the x and y axes, that is, open conditions. On the other hand, on the z axis a short-circuit condition is chosen, that is electrical wall, at the lower limit. And a radiation condition, or add-space condition, at the upper limit since that zone will be the radiation area, that is where the antenna radiates.

(a) Slots layout in CST

(b) CP-RLSA designed in CST with an open-circuit ending
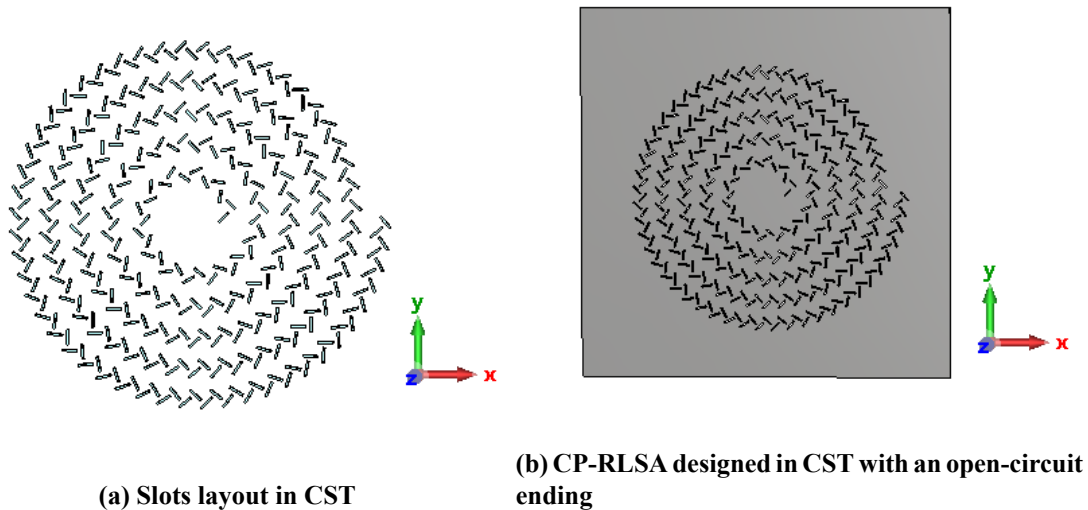
Figure 2.3: Plain view of the slots representation and CP-RLSA in CST

After having defined the boundary conditions, as well as the port, the simulation of the antenna at a frequency of 30 GHz will be carried out. Furthermore, the far-field monitors (Field monitor) must be set in this case to obtain the radiation patterns. In addition, electric and magnetic field monitors can be established in case the electric or magnetic field of the antenna needs to be studied.
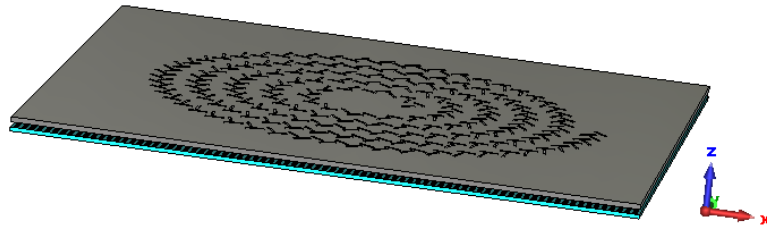
Figure 2.4: CP-RLSA in CST

In Fig. 2.4, a preview of the RLSA antenna can be seen where the part corresponding to the distribution of patches and the upper cover with the slots are exemplified. That distribution of patches corresponds to the metasurface which will be studied in detail in the next chapter. Moreover, the open circuit conditions on the x and y axes is distinguishable. In Fig. 2.5 the phase of the z-component of the electric field can be seen and as will be explained later, the electric field has to propagate radially to ensure the correct performance of the antenna. Thus, analyzing this phase is essential when analyzing the operation of the antenna.
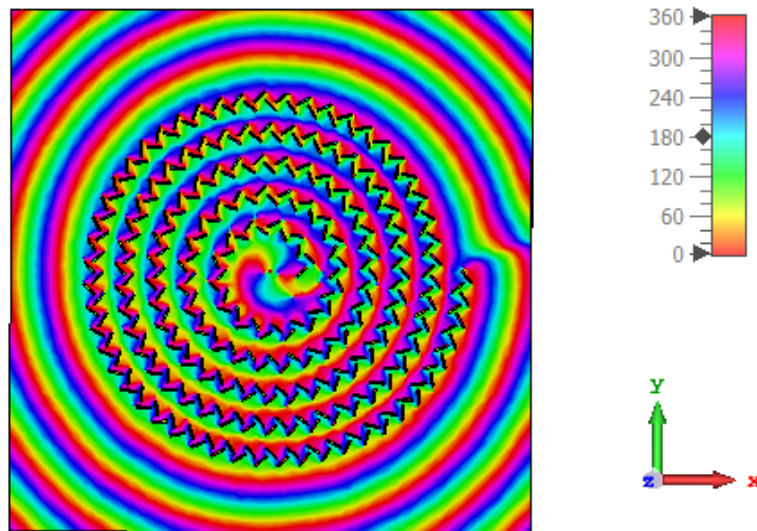
Figure 2.5: Phase representation of z component of the electric field in CST

Additionally, in Fig. 2.6, once it has been verified that the electric field is propagating radially, it can be seen in which direction the maximum of the radiation pattern points analyzing its 3D representation. In this way it is attested that the main lobe points towards the correct angle according to the previously designed antenna. The maximum of the radiation pattern is located at $\theta = 0°$ in this case.

As can be seen in Fig. 2.6, due to the established boundary conditions, the values presented in the pattern cover a θ range between -90º and 90º.
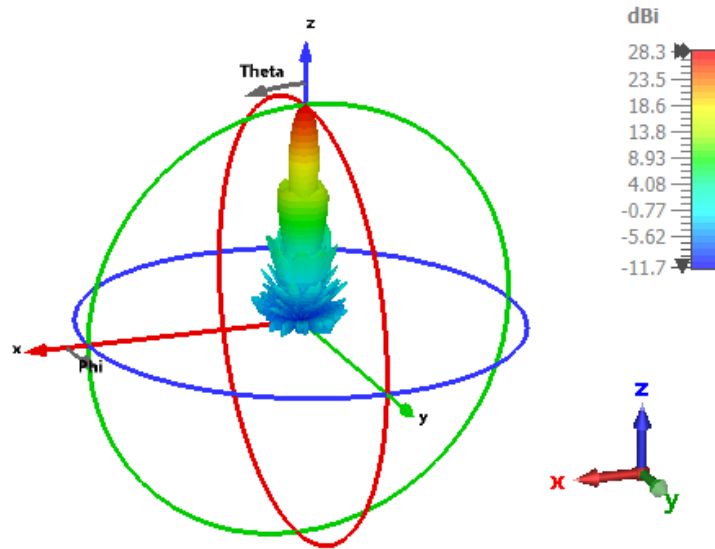
Figure 2.6: 3D representation of a CP-RLSA radiation pattern with a 0º tilt

2.4   Beam-steering methods

As defined at the beginning of this project, the objective of this antenna is to find the ability to communicate either with several satellites or from different fixed points with a single moving satellite. Specifically, the idea is to ensure that the antenna can reach various inclinations without having to physically move the antenna. For this reason, this section will follow the steps taken in [15] where two topologies of the same antenna are taken as an example and contrasted for the cases in which a tilt of 0º (broadside case) and 10º are represented. In this study, a similar analysis will be carried out, but changing certain parameters due to the fact that the computational cost is much higher in this case due to the metasurface characteristics. Therefore, the distribution of slots will have a total of N = 5 turns around the upper plate and not N = 8 as shown in [15]. Thus, two antennas with a tilt of 0º and 10º respectively will be contrasted.

As specified in [15], in order to achieve a beam steering value other than 0º as regards the initial antenna (broadside) a variation in the phase of the electric field must be forced between the different pairs of slots. As can be seen in Fig. 2.7, the phase of the field is almost uniform (Fig. 2.7a) and therefore the direction of the beam is perpendicular to the structure (broadside), while in the other example, the representation of the phase seems to follow a linear variation (Fig. 2.7b). It should be noted that the term tilt refers to the difference that exists between the steering of the main beam of the antenna and the direction $\theta = 0$ (broadside).

(a) Broadside design   (b) 10º tilt
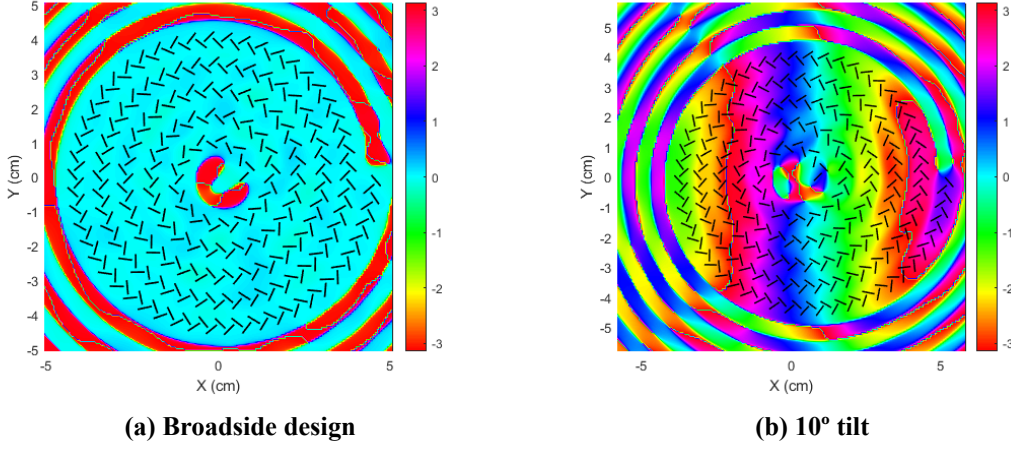
Figure 2.7: Phase of the z-component of the electric field in teh aperture

Therefore, in this section two methods of antenna steering are described, the first one referring to the alteration of the position of the slots, and the second one associated with the guide permittivity which will be variable and will cause that inclination.

2.4.1 Variation of slots spacing

This section defines how the beam-steering can be formed by changing the configuration of the slots. Previously, it has been briefly explained how the design and generation of the slots take place, which is nothing more than a variation of the phase with respect to the copolar component of the electric field. The aim of this project is to maintain the existing spacing between pairs of slots along the y axis, in the same way that the distance between the turns of the semi-axis x- decreases, while it increases in x +.

Another more mathematical way of looking at the relationship between the spacing, which will be called S_ρ, and the pointing angle is shown in the equation:

$$S_\rho = \frac{\lambda_g}{1 - \frac{1}{\sqrt{\epsilon_r}} \sin(\theta_T) \cos(\phi' - \phi_T)} \tag{2.2}$$

The distribution of slots as shown in Fig. 2.8, is implemented making use of a provided Matlab file and developed in [10] at the UPV. With this program, it is possible to generate a distribution of slots for a CP-RLSA design with parametrizable beam-steering values, that is, the coordinates ϕ_T and θ_T will be variable. Notwithstanding, in this case, only θ_T will be variable since the slot spacing on the y axis will be constant ($\phi_T = 0$).
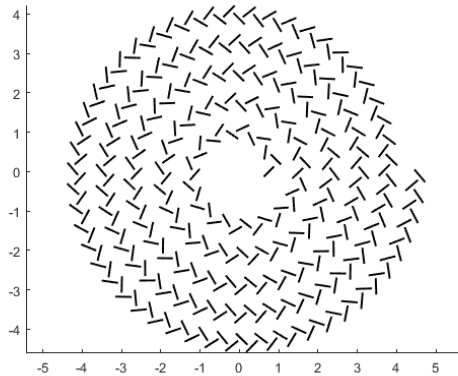
Figure 2.8: Broadside slots distribution in Matlab

In Fig. 2.8 it can be seen how the distribution of slots around the center is uniform and does not show any variation. Whereas, in Fig. 2.9, the representation of the slot is no longer uniform. Although in the left part, the slots are closer to each other, and in the right part a greater spacing between them is observed, presenting an asymmetric distribution, corroborating the initial statement.
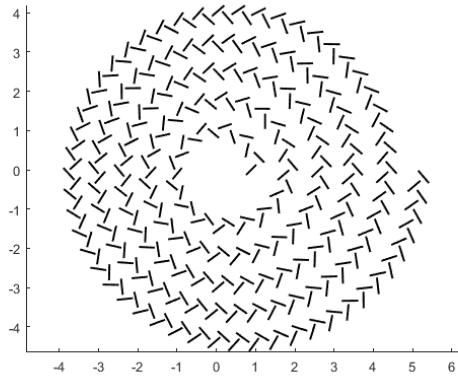
Figure 2.9: 10º tilt slots distribution in Matlab

2.4.2 Variation of permittivity

The objective consists of ensuring that each point forming the radial waveguide has a different permittivity value, in such a way that different electrical wavelengths are obtained in the waveguide. Thus, phase control is achieved due to the different speeds of the propagation wave, the linear phase shift achieved, is what causes a tilted beam. The association of different values of permittivity will be carried out with a metasurface, which will be seen in more detail in later chapters. It consists of patches and mushroom-like structures on a grounded dielectric slab. For each permittivity value, a different patch width will be obtained. This permittivity will be calculated according to equation (2.2).

As said before, S_ρ is the spacing between the slots and θ_T and ϕ_T are the spherical coordinates in which the maximum of the beam will be defined. As studied in the previous section, ϕ_T will be set to zero since the beam-steering will take place on the XZ-plane.

Likewise, the relative permittivity will be solved in the Equation (2.2), in order to achieve a permittivity value according to a tilt value, forming the Equation (2.3).

$$\varepsilon_r(\phi) = \left(\frac{\lambda_0}{S_\rho} + \sin(\theta_T)\cos(\phi') \right)^2 \tag{2.3}$$

From equation (2.3) it can be extracted that the maximum permittivity will take place in plane $\phi' = 0$. Additionally, when ϕ' reaches a value of 180º, the permitivities will be minimum, that is, $\cos(\phi' = 180º)$ = -1. Then, the highest values of permittivity will occur in the positive direction of the x semi-axis.

Fig. 2.10a and Fig. 2.11a show two patches distributions for the broadside case and for a tilt of 10º. In Fig. 2.10a the patches are all equipped with the same size, forming a uniform distribution, as was the case with the slots. On the other hand, Fig. 2.11a shows a distribution of patches of different sizes so that a main beam inclination can be achieved. However, in both cases the slots will have a uniform distribution, since in this method the patches are what cause the beam to have a certain inclination and not the slots as in the previous method.

This distribution of patches has been carried out through the implementation of a Matlab code in which a grid is created and following Equation (2.3), a permittivity value is associated to each cell of the grid, translating this later to CST into different values of patch width.

(a) Distribution of patches 0º tilt

(b) Distribution of slots 0º tilt
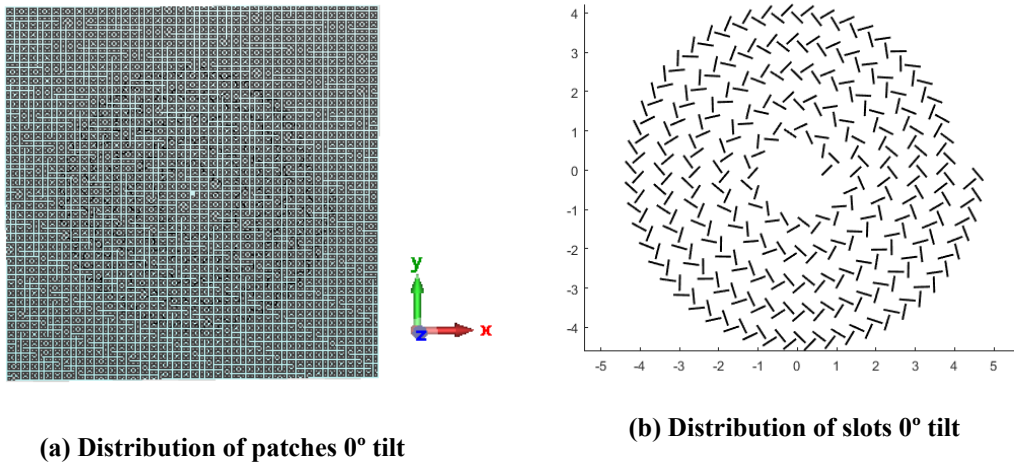
Figure 2.10: Broadside slots and patches distribution

(a) Distribution of patches 10º tilt

(b) Distribution of slots 0º tilt
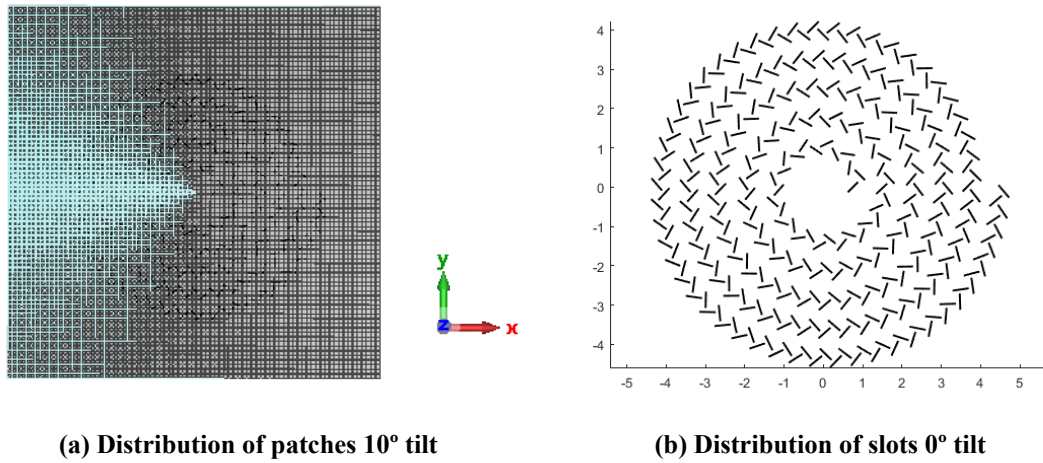
Figure 2.11: Slots and patches distribution 10º tilt

(a) Detailed broadside distribution of patches

(b) Detailed distribution of slots 10º tilt
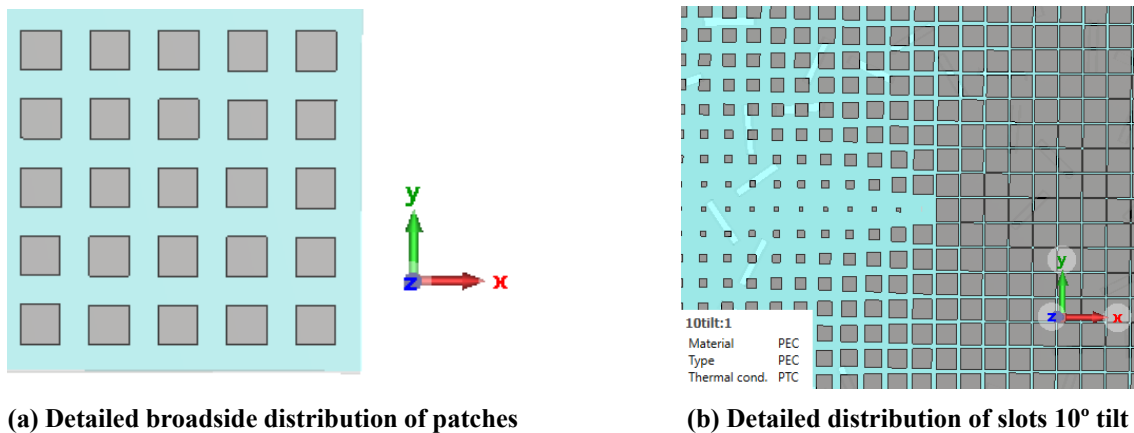
Figure 2.12: Detailed patches distribution for 0º and 10º tilt

2.4.3 Rotating upper plate

In this section the theoretical process will be defined in relation to the effects caused by combining a metasurface with a certain tilt value together with a distribution of slots with the same inclination, in order to multiply the final angle by two. In addition, emphasis will be placed on the result of rotating one of the waveguide plates as previously mentioned, in this case the rotation of the upper plate containing the slots will be done, and the study of what angle should be achieved using that rotation. Finally, the results found in CST will be shown and a comparison with the theoretical model will be established.

An analysis based on [15] will be carried out in which the mathematical foundation for a pin structure is established. In this case, this foundation will be applied to the metasurface made with patches and the Equation (2.3) will be taken up and applied to the models considered for this study. The Equation (2.4) establishes the variation of the spacing between the pairs of slots of the upper

plate as a function of the angular position (ϕ'), that they occupy in cylindrical coordinates, that is, the radial spacing. This spacing causes the beam to be displaced $(\theta_s - \phi_s)$ with the design of a constant patch distribution over the dielectric, in which ε_{rs} is defined as the equivalent relative permittivity in the guide.

$$S_\rho(\phi') = \frac{\frac{\lambda_0}{\sqrt{\varepsilon_{rs}}}}{1 - \frac{1}{\sqrt{\varepsilon_{rs}}}\sin(\theta_s)\cos(\phi' - \phi_s)} \tag{2.4}$$

In addition, the Equation (2.5) will be taken into account to this time point the beam in the direction (θ_E, ϕ_E) in such a way that the equivalent permittivity is modified as a function of the angular position (ϕ') in cylindrical coordinates, $S_{\rho E}$ is defined as the spacing between pairs of slots.

$$\sqrt{\varepsilon_r}(\varphi') = \frac{\lambda_0}{S_{\rho E}} + \sin(\theta_E)\cos(\varphi' - \theta_E) \tag{2.5}$$

The Equations (2.4) and (2.5) refer to the CP-RLSA designs when two different antenna implementation models mentioned below were taken into account:

- Methodology 1: Configuration of rings for a given tilt and a distribution of patches with a constant permittivity (all patches have the same size) (1)

- Methodology 2: Configuration of rings for a broadside case and a distribution of patches with a variable permittivity (the size of the patches changes according to the formula) (2)

As mentioned above, an analisys of the behavior of the antenna when the rings of the first methodology are combined in the same design together with the distribution of patches of the second will be studied. In the first equation the spacing parameter $S_\rho(\phi')$ has been calculated by means of an offset (θ_s, φ_s) for a fixed relative permittivity value ε_{rs}. On the other hand, the size of the patches has been designed for a specific pointing (θ_E, φ_E) taking into account a constant spacing $S_{\rho E}$. The pointing direction $(\theta_0, \varphi_{-}0)$ referring to a array provided by a certain spacing and permittivity as a function of the angular position (ϕ') of the pair of slots, is defined by the Equation 2.6.

$$\sin(\theta_0)\cos(\varphi' - \phi_0) = \sqrt{\varepsilon_r} - \frac{\lambda_0}{S_\rho} \tag{2.6}$$

In the Equation 2.6, the value of the spacing S_ρ between the slots, belongs to the design of constant patch size (1), and the permittivity is given by the design of variable patch size (2). In this way it is established that:

$$\sin(\theta_0)\cos(\varphi' - \phi_0) = \frac{\lambda_0}{S_{\rho E}} + \sin(\theta_E)\cos(\varphi' - \phi_E) - (\sqrt{\varepsilon_{rs}} - \sin(\theta_s)\cos(\varphi' - \phi_s)) \tag{2.7}$$

$$\sin(\theta_0)\cos(\varphi' - \phi_0) = (\frac{\lambda_0}{S_{\rho E}} - \sqrt{\varepsilon_{rs}}) + \sin(\theta_E)\cos(\varphi' - \phi_E) + \sin(\theta_s)\cos(\varphi' - \phi_s) \tag{2.8}$$

As stated in [15], the expression (2.9) must be fulfilled for any value of (ϕ'), therefore:

$$\sqrt{\varepsilon_{rs}} = \frac{\lambda_0}{S_{\rho E}} \tag{2.9}$$

Therefore, the design of the slots using Matlab has to be done considering the permittivity that is used when the variable patch distribution is generated, thus leaving the pointing equation shown in Equation 2.10.

$$\sin(\theta_0)\cos(\varphi' - \phi_0) = \sin(\theta_E)\cos(\varphi' - \phi_E) + \sin(\theta_s)\cos(\varphi' - \phi_s) \tag{2.10}$$

Equation (2.10) is reformulated as:

$$\sin(\theta_0)[\cos(\varphi')\cos(\phi_0) + \sin(\varphi')\sin(\theta_0)] = \sin(\theta_E)[\cos(\varphi')\cos(\phi_E) + \sin(\varphi')\sin(\theta_E)]$$
$$+ \sin(\theta_s)[\cos(\varphi')\cos(\phi_s) + \sin(\varphi')\sin(\phi_s)$$

So, if the dependence is separated into sine and cosine, it remains:

$$\sin(\theta_0)\cos(\phi_0) = \sin(\theta_s)\cos(\phi_s) + \sin(\theta_E)\cos(\phi_E) \tag{2.11}$$

$$\sin(\theta_0)\sin(\phi_0) = \sin(\theta_s)\sin(\phi_s) + \sin(\theta_E)\sin(\phi_E) \tag{2.12}$$

From the previous equations, the pointing in elevation and azimuth is defined as:

$$\sin^2(\theta_0) = [\sin(\theta_s)\cos(\phi_s) + \sin(\theta_E)\cos(\phi_E)]^2 + [\sin(\theta_s)\sin(\phi_s) + \sin(\theta_E)\sin(\phi_E)]^2 \tag{2.13}$$

$$\tan(\phi_0) = \frac{\sin(\theta_s)\sin(\phi_s) + \sin(\theta_E)\sin(\phi_E)}{\sin(\theta_s)\cos(\phi_s) + \sin(\theta_E)\cos(\phi_E)} \tag{2.14}$$

The previous equations can be applied in different cases such as:

1. Same elevation and azimuth angle: $\theta_s = \theta_E$ and $\phi_s = \phi_E$

$$\sin^2(\theta_0) = 4\sin^2(\theta_s), \sin(\theta_0) = 2\sin(\theta_s) \tag{2.15}$$

$$\tan(\phi_0) = \tan(\phi_s), \phi_0 = \phi_s \tag{2.16}$$

In this case the elevation angle is multiplied by 2.

2. Same elevation angle and azimuth angle is rotated 180º: $\theta_s = \theta_E$ and $\phi_s = \phi_E + \pi$

$$\sin^2(\theta_0) = 0, \sin(\theta_0) = 0 \tag{2.17}$$

In this case, the beam-steering would be 0 (broadside)

3. Same elevation angle and azimuth angle is rotated an arbitrary angle: $\theta_s = \theta_E$ and $\phi_E =$

$\phi_s + \alpha$

$\sin^2(\theta_0) = \sin^2(\theta_s) \left[\cos(\phi_s) + \cos(\phi_s + \alpha)\right]^2 + \sin^2(\theta_s) \left[\sin(\phi_s) + \sin(\phi_s + \alpha)\right]^2$

$= \sin 2(\theta_s) \left[2 + 2\cos(\phi_S)\cos(\phi_s + \alpha) + 2\sin(\theta_s)\sin(\phi_s + \alpha))\right]$

$= \sin^2(\theta_s) \left[2 + \cos(\alpha) + \cos(2\phi_s + \alpha) + \cos(\alpha) - \cos(2\phi_s + \alpha)\right]$

$= 2(1 + \cos(\alpha))\sin^2(\theta_s)$

$tan(\phi_0) = \frac{\sin(\phi_s)\sin(\phi_s+\alpha)}{\cos(\phi_s)+\cos(\phi_s+\alpha)} = \frac{\sin(\phi_S)+\sin(\phi_s)\cos(\alpha)+\cos(\phi_S)\sin(\alpha)}{\cos(\phi_s)+\cos(\phi_s)\cos(\alpha)+\sin(\phi_s)\sin(\alpha)} = \frac{tan(\phi_s)+\frac{\sin(\alpha)}{1+\cos(\alpha)}}{1-tan(\phi_s)\frac{\sin(\alpha)}{1+\cos(\alpha)}}$

$$\phi_0 = \phi_s + tan^{-1}\left(\frac{\sin(\alpha)}{1+\cos(\alpha)}\right)$$

For instance, if the arbitrary angle were $\frac{\pi}{2}$, the beam-steering angle would be:

$$\sin^2(\theta_0) = 2\sin^2(\theta_s) \tag{2.18}$$

$$\phi_0 = \phi_s + \frac{\pi}{4} \tag{2.19}$$

Chapter 3

Study and design of a metasurface

In this chapter the analysis of the metasurface using patches and mushrooms will be carried out. CST Microwave studio will be used in order to simulate and study the dispersion diagrams of each structure and to design the unitary cell which will be used to create the metasurface.

3.1 Metamaterials

Traditionally, the internal structure of different antennas used to be formed by either a dielectric of a determined permittivity, or by layers of the same dielectric. Both structures allow the field to propagate through the waveguide. However, a new type of material arises that can replace in most cases this internal structure formed by dielectrics, with the peculiarity that unlike what happens with the dielectric, the characteristics of this new material called metamaterial do not depend on its own composition but on its form. That is, generally, metamaterials are periodically molded into a surface. When this surface is generated in two dimensions, it is usually called a metasurface. Metamaterials have had a great impact in different fields such as photonics, where in [16] the characteristics for recent metasurface applications for flat optical devices are collected and, as specified, the metasurfaces are useful for designing different types of properties such as amplitude, phase, and polarization. As a matter of fact, it is possible to carry out a large number of flat optical devices such as holograms for the generation of beam vector [17].

There is a type of metasurface called EBG (Electromagnetic Bandgap) on which the type of metasurface used during this project will be based. This EBG is made up of two plates, a completely metallic upper one and a metallic lower one that will also include the periodic metasurface. A remarkable characteristic is that this structure can achieve a range of frequencies in which the electromagnetic waves stop propagating. Moreover, different studies and passive devices in the microwave and millimeter bands have been carried out based on this EBG structure [18] [19] due to their importance in the field of antennas.

General dispersive characteristics of a metasurface are given by its repeating unit cell. Depending on this unit and how it is arranged, we will find different behaviors in their respective propagation modes.

In this project, a metasurface made up of patches and mushrooms will be studied.

3.2 Dispersion diagram

Dispersion diagram is an existing graphical relationship that shows the dependence with frequency of the wavenumber or propagation constant of a wave propagating through a certain medium. In the case of free space $\varepsilon_r = 1$, any electromagnetic wave in that medium will propagate at the same speed regardless of its frequency. It is also often said that dispersion diagram consists of a line increasing along with frequency, which is also called a Light Line and is represented in Fig. 3.1. In the following sections, dispersion diagram is modified simply by playing with the topology and geometry, mostly of the unit cell, so that the desired propagation constant is obtained.
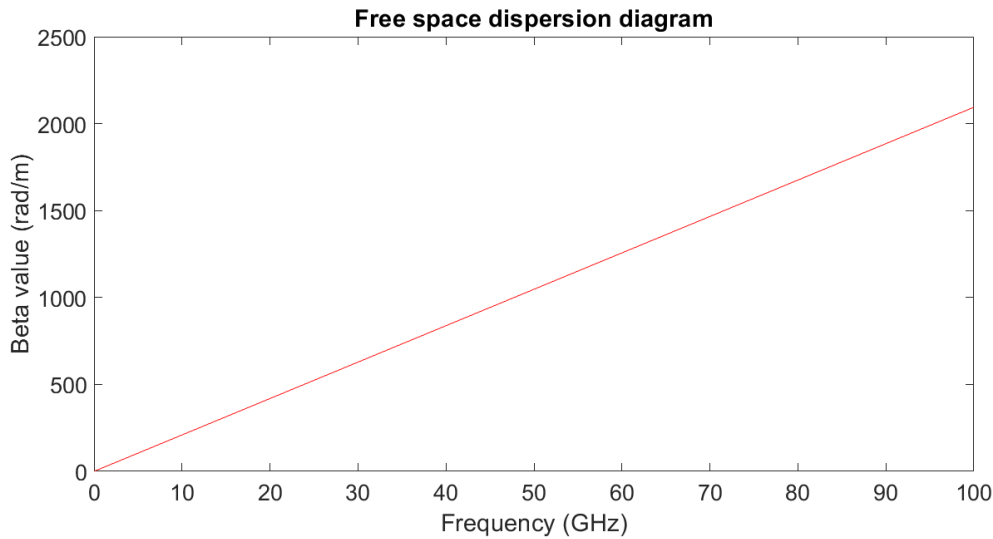
Figure 3.1: Free space dispersion diagram in Matlab

3.3 Unit Cells

As previously mentioned, metamaterials are a type of material that cannot be found naturally, and their usefulness does not lie in their properties but in their structure. Therefore, in order to carry out a metasurface and, consequently, to achieve the appropriate one for the implementation of the RLSA antenna studied throughout this project, different types of structures could be considered and used as an alternative to a dielectric.
In [15] the structure used was based on a pin model. Those pins were found in cells of a size of around 2 mm and 2.5 mm, the height of the waveguide was 3 mm and 4 mm, depending on the study, being the pins the only structure used and with either a constant or a variable height. This antenna presented highly satisfactory results since it was able to reach beam-steering angles up to 20º, although with 20º the directivity is affected, as well as the SLL. It can be said that the antenna attains the expected objectives.

In the case of the metasurface considered in this project, it is made up of patches and mushrooms, some of them slotted. This implies that the simulation time will be longer because a permittivity value and cell size which satisfy the 3 structures must be found in order to combine them and thus obtain a greater range of permittivity.

In a first study, the analysis of 3 different structures will be carried out for different values of permittivity and cell size: patches, simple mushrooms and slotted mushrooms. Mushroom structures will be based on a study carried out in [20]. The aim of the study is to find a table with information regarding patch width, propagation constant β and therefore, effective permittivity ε_{eff}. Furthermore, boundary conditions are established as: magnetic walls in x+ and x-, electric wall in y+ and y- and periodicity in z+ and z-, simulating the parallel-plate waveguide characteristics containing patches or mushrooms.

General features for the three structures are established as:

- p : standard cell size (period)

- h_s : substrate height

- h_g : waveguide height

(a) Patch   (b) Simple mushroom   (c) Slotted mushroom
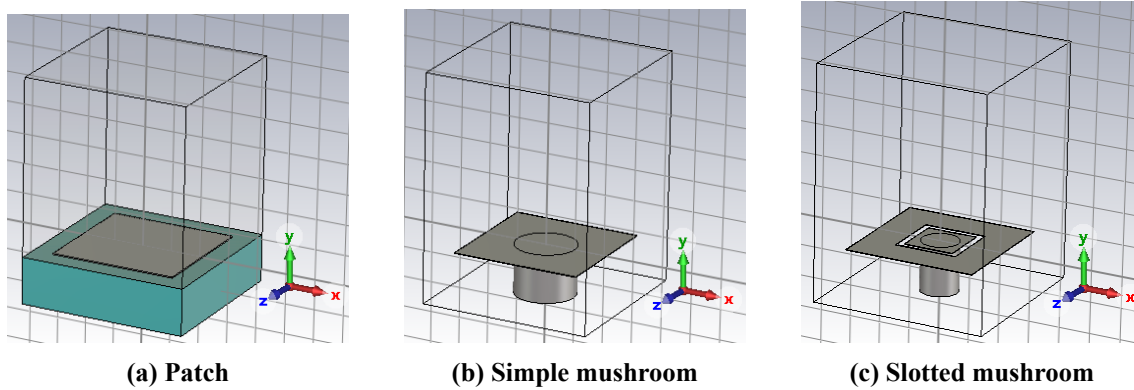
Figure 3.2: Unit cell structures

As can be seen in Fig. 3.2 the three structures to determine the metasurface are introduced. the first one in 3.2a consists of a slice of square PEC material lying on a dielectric and as can be seen it is the simplest structure. In the case of simple mushrooms, the patch structure will be exactly the same, but adding a cylinder inside of the dielectric under the patch as shown in Fig. 3.2b. As regards slotted mushrooms, this structure follows the features of the simple mushroom, but a slot is added contouring the patch and has a thickness of 0.1 mm, although this value can be changed in order to reach higher permittivity values.

3.3.1 Wave propagation in radial waveguide

The propagation constant in a waveguide, and concretely a parallel-plate waveguide in this case, of a certain mode shows the variation of the phase along the propagation direction at a de-

termined frequency (30 GHz). This constant can be defined as shown in (3.1) where α is the attenuation coefficient and β the phase constant.

$$\gamma = \alpha + j\beta \tag{3.1}$$

The antenna has been designed considering metallic plates which are PEC (Perfect Electric Conductor), and since the dielectrics are considered to be ideals and without losses, that is $\alpha = 0$. Propagation constant will be defined as (3.2).

$$\gamma = j\beta \tag{3.2}$$

Hence, the phase constant can be considered to be proportionate to the wavenumber, k, of a plane wave. The equation of such can be found in (3.3), where $\mu_r = 1$, due to the environmental conditions, and ε_r is the permittivity inserted inside the radial waveguide.

$$\beta = k = \omega\sqrt{\mu_0 \mu_r \epsilon_0 \epsilon_r} = \frac{\omega}{c_0}\sqrt{\epsilon_r} \tag{3.3}$$

Notwithstanding, in this work, finding a value for the propagation constant is not as simple as considering (3.3), since the waveguide is not filled with a homogeneous dielectric but a distribution of patches and mushrooms. Consequently, a study will be carried out to analyze the variations of the propagation constant for this model. This study is simply based on observing the electromagnetic behavior of the patches and mushroom structure. In order to achieve this behavior and be able to study it, the Eigensolver mode of the software CST will be used to simulate either a patch or a mushroom in a unitary cell as explained previously. The aim of this module is to resolve the wave equation inside the structure, providing the propagating modes for the operation frequency, and therefore the dispersion diagram for each of them, as well as other curves. In this case, the TEM mode is the one considered.

In order to analyze properly all of this, several ideas must be taken into account, the first one would be that the field distribution is periodic in the whole structure. Moreover, each cell provoke a phase-shift. This phase-shift will depend on β value solutions reached after simulating each structure, which goes along with the value of the periodicity of the cell, p. As patches and mushrooms present symmetric structures, phase-shift values in x and z axes will be the same, that is $\phi_x = \phi_z$, and where $\phi_x = k_x p$ and then $\phi_z = k_z p$. That means that the phase-shift value corresponding to the incident wave when the inclination is 0º, is the same value for a wave which arrives with a perpendicular inclination, 90º. Thus, propagation constant can be defined as:

$$\beta = \sqrt{k_x^2 + k_z^2} \tag{3.4}$$
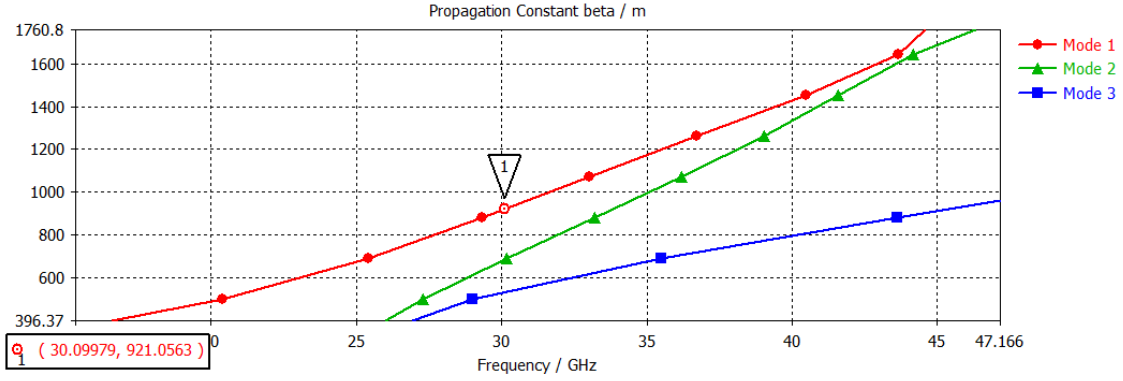
Figure 3.3: Dispersion diagram in CST

After having simulated the periodic structure with the specified boundary conditions using the Eigensolver module on CST, the dispersion diagram can be found as well as other curves as said before. An example of such is shown in Fig. 3.3 where the curves are associated to each propagating mode inside the waveguide.

As can be seen, at a frequency of 30 GHz, i.e., central frequency of the antenna, there are three propagating modes. However, there should be only one (fundamental mode) to ensure the well-functioning of the antenna. In the case of Fig. 3.3 Mode 1 is the fundamental mode.

In order to realize an analysis of the metasurface, each type of structure must be studied separately to obtain the appropriate cell width, guide height, substrate height, and permittivity characteristics to provide a metasurface that complies with the established requirements, which basically consist of the electric field propagating radially and, furthermore, being capable of causing a beam-steering. The study of each structure is carried out independently in CST starting from some initial values and observing the dispersion diagram which is similar to the one shown in Fig. 3.3. The simulation is carried out using the Eigensolver option in CST, having previously selected the boundary conditions explained in this section.

3.3.2 Study of structures

In this section each structure will be studied as previously defined. The objective is to find a range of values of β between $600 \frac{rad.}{m}$ and $1200 \frac{rad.}{m}$. Such range corresponds to permittivity values ranging from 1 to 3.5, approximately, as $\varepsilon_r = \left(\frac{\beta}{\frac{2\pi}{k}} \right)^2, k = \frac{c_0}{f}$.

3.3.2.1 Patches simulation

Starting from the initial features:

- $p = 2.5$ mm

- $h_g = 3.5$ mm

- $h_s = 0.508$ mm (according to dielectric width standards)

A structure like the one shown in Fig. 3.4 is obtained.
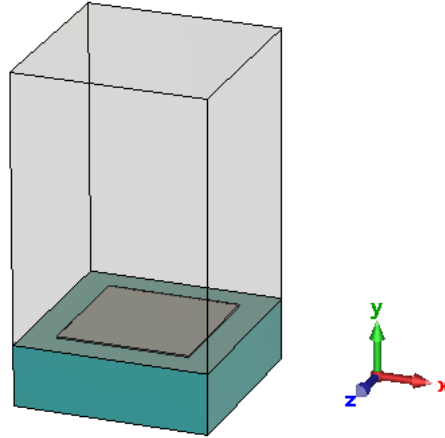
Figure 3.4: Patch structure

In Fig. 3.4, the arrangement of the patch placed on the dielectric block can be seen. A study of the dispersion diagrams resulting from changing the permittivity value of that dielectric block must be carried out (substrate permittivity).

As a first test, a substrate permittivity value of 1.5 is chosen, but the range of values of β oscillates between 643.6 and 651 for different patch sizes when, as previously mentioned, a range similar to 600-1200 in terms of β values must be reached in order to implement a metasurface with a large variety of patch sizes and reach higher beam-steering values.

Distance between patches (mm)	β value
0.2	651
0.3	650
0.8	645
1.8	643
2.2	643.6

Tabla 3.1: CP-RLSA Design parameters

Then the initial value of 1.5 will be increased to reach a reasonable range.

For the case of a permittivity value of 4, Table 3.2 shows the interval of β values for different patch widths. As can be seen, this is a highly positive range that could offer good performance.

Distance between patches (mm)	β value	ε_{eff}
0.2	Out of range	/
0.3	1190.4	3.59
0.5	935.6	2.22
1	701.8	1.25
1.5	676.4	1.16
2	673	1.15
2.3	670.8	1.4
2.4	670	1.4

Tabla 3.2: CP-RLSA Design parameters

The effective permittivity has been found according to the already mentioned equality (3.5).

$$\varepsilon_{eff} = \left(\frac{\beta}{\frac{2\pi}{k}} \right)^2 , k = \frac{c_0}{f} \tag{3.5}$$

Therefore, for the initial features established, with a perimittivity value of 4 the structure offers positive results.

3.3.2.2 Simple mushrooms simulation

In this case, the permittivity value of 4 found in the previous section will be maintained so that the values of the structure and cell will be alternated to find the range of values of β.

The dimensions of the simple mushroom are defined as follows:

- **Cylinder height**: 0.508 mm

- **Cylinder radius**: 0.3 mm
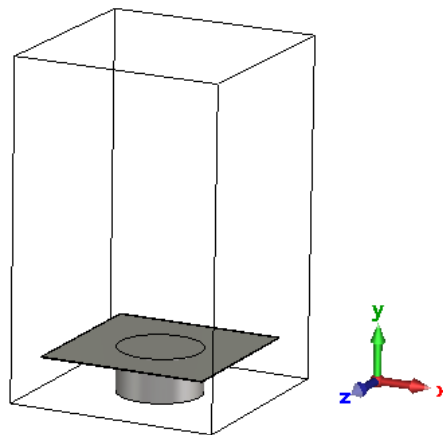
Figure 3.5: Simple Mushroom structure

In this case, the values of period and waveguide height are alternated taking into account the same value of substrate height and permittivity used in the case of the simple patches, to get the dimensions of the structure which provides the best β range.

After carrying out several studies it has been determined that the features that offer better results are:

- p: 2.2 mm

- h_s: 0.508 mm

- h_g: 3.5 mm

Those parameters are the same as the ones used during the patch structure excluding the period value which is lower.

The resulting table can be found below:

Distance between patches (mm)	β value	ε_{eff}
0.2	905	2.075
0.3	751	1.429
0.4	710	1.277
0.5	693	1.216
0.6	684	1.185
0.7	676	1.157
0.8	670	1.137
0.9	666	1.124
1	662	1.110

Tabla 3.3: CP-RLSA Design parameters

3.3.2.3 Slotted-mushrooms simulation

First, the main dimensions of the structure will be established as before:

- **Cylinder height**: 0.508 mm

- **Cylinder radius**: 0.3 mm

- **Slot width**: 0.1 mm

In this case, the analysis will be more detailed as there are more parameters to take into account such as the slot located in the patch of the mushroom, this slots width value will be considered as 0.1 mm at first and will be modified in order to achieve higher or more specific values of β while studying the dispersion diagram.
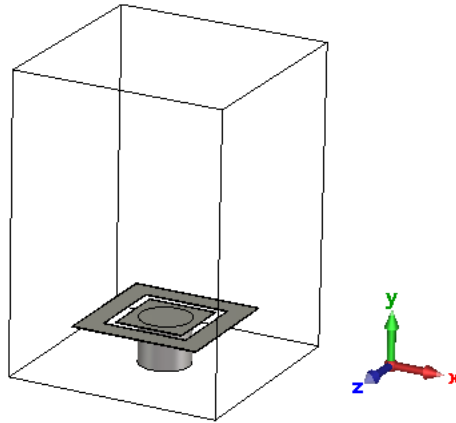
Figure 3.6: Patch structure

Starting from the previous characteristics for a period of 2.2 mm as considered in the case of simple mushrooms, a substrate height of 0.508 mm and a permittivity value of 4, the results for this structure are obtained as follows:

Distance between patches (mm)	β value	ε_{eff}
0.2	726	1.335
1	671	1.140

Until now, a substrate width of 0.508 mm had been considered, but judging by the results found, other normalized substrate heights such as 0.787 mm and 1.575 mm will be tested to see what happens in these cases.

Considering a substrate height of 1.575 mm, the fundamental mode does not propagate at a frequency of 30 GHz
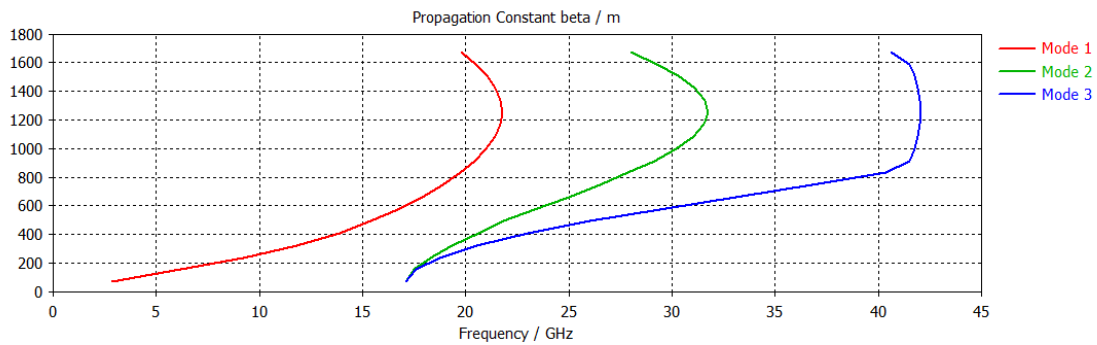
Figure 3.7: Dispersion diagram h_s = 1.575 mm and p = 2.5 mm

For the case in which a substrate height of 0.787 mm is considered, the table results as follows:

Distance between patches (mm)	β value	ε_{eff}
0.2	902	2.061
0.8	740	1.387
1	724	1.328

As can be seen, the interval is reduced, so the size of the period will be increased to see if higher values of β can be reached. For the case in which the period has a width of 2.8 mm:

Distance between patches (mm)	β value	ε_{eff}
0.2	1109	3.115
1.6	708	1.270

This interval is the one with the best performance since, as can be seen in Fig. 3.8, for a frequency of 30 GHz the maximum value that β can reach is obtained.
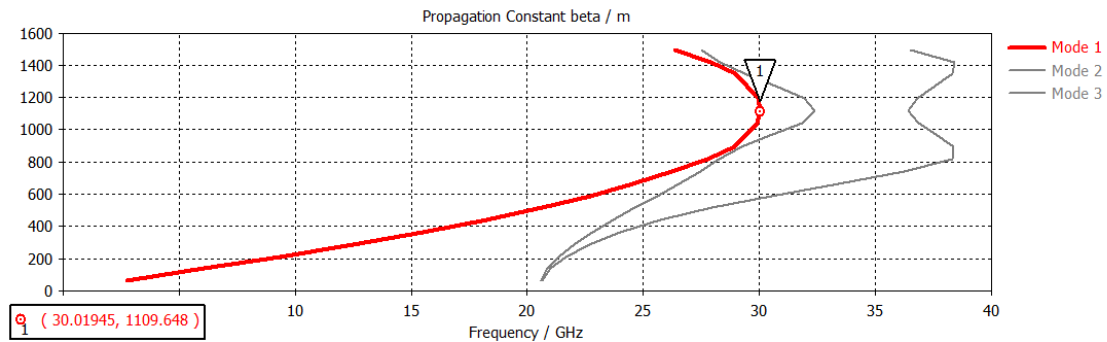
Figure 3.8: Slotted mushroom dispersion diagram example

3.3.3 Unit Cell Conclusions

After evaluating the three structures and finding an interval of values of β for each one of them, we proceed to determine cell dimensions that will be common to all the structures in order to implement the metasurface. Since the slotted mushroom structure is the most complex, the period and substrate height values found for this structure will be used.

- p = 2.8 mm

- $\varepsilon_r = 4$

- h_g = 3 mm

- h_s = 0.787 mm

Therefore, patches and simple mushrooms structures will be simulated again under these characteristics and the resulting final table is the one indicated below:

| Permittivity (mm)	β value	Type of element
1.15	674	Patch
1.16	678	Patch
1.21	692	Patch
1.25	703	Slotted-Mushroom
1.27	708	Slotted-Mushroom
1.28	712	Simple Mushroom
1.37	735	Patch
1.39	740	Slotted-Mushroom
1.46	759	Simple Mushroom
1.72	825	Slotted-Mushroom
1.86	856	Slotted-Mushroom
2.71	1035	Simple Mushroom
3.12	1109	Slotted-Mushroom

The table shows that simple mushrooms do not provide a large value range of β, so they can be put aside. In addition, more patch and slotted mushroom values will be calculated in order to avoid large gaps between permittivity values. The readjusted table without simple mushrooms results as follows:

Permitivitty (mm)	β value	Type of element	Patch width (mm)
1.15	674	Patch	0.8
1.16	678	Patch	1.3
1.21	692	Patch	1.8
1.23	696	Patch	1.9
1.25	703	Patch	2
1.29	715	Patch	2.1
1.32	722	Patch	2.2
1.37	735	Patch	2.3
1.39	740	Slotted-Mushroom	1.8
1.49	766	Slotted-Mushroom	2
1.54	780	Slotted-Mushroom	2.1
1.63	801	Slotted-Mushroom	2.2
1.72	825	Slotted-Mushroom	2.3
1.86	856	Slotted-Mushroom	2.4
2	889	Slotted-Mushroom	2.5
2.23	938	Slotted-Mushroom	2.5
2.52	998	Slotted-Mushroom	2.45
3.12	1109	Slotted-Mushroom	2.6

Tabla 3.4: Patch width values depending on permittivity

This table is the one that will be used in Matlab to create a grid in which each cell will be assigned a permittivity value following formula (2.3), starting from a value of tilt and a value of S_ρ. The value of S_ρ is obtained by adjusting Equation (2.2), that is, S_ρ provides the interval of permittivities for different tilt values for the cases in which $\phi \in (0, 90)$. This interval must be

within the range of permitivities in the previous table. The result in Matlab is shown in Fig. 3.9.
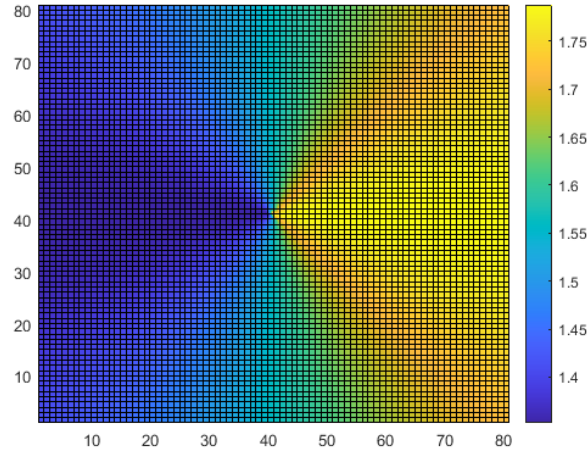
Figure 3.9: distribution of permittivity values in a grid using Matlab

Where a radial distribution of permittivities is observed. Such distribution will be saved in a .txt file and interpreted by a CST program where either a patch or a slotted mushroom will be designed for each cell depending on the permittivity according to Table 3.4.

In the following studies, the analysis are carried out for the initial values of cell size and guide height:

- p : 2.8 mm

- λ_0 : 10 mm

- Antenna radius : $3\lambda_0$

3.3.4 First study: $p = 2.8$ mm and $h_g = 3$ mm

After obtaining the data of effective permittivities ε_{eff} and size of patches and mushrooms described during the previous section in Table 3.4, the simulation of the complete structure will be processed, which will be formed by patches with a size of 30x30 cells to lessen the simulation time, a dielectric which permittivity value will be 4 and its width 0.787 mm, and finally the upper platform. This platform is the one that contains the slots, but at first these will not be considered since the efficiency of the propagation of the electric field through the antenna must be analyzed first and once satisfactory results have been obtained, the slots are included and simulated with far field conditions.

Therefore, when analyzing the field, the appropriate conditions are established for this as the electric field condition in the z- and z + directions and the open condition in x-, x +, y-, y +. In addition, the port location is set to a central position within the guide and also the Field Monitor is considered to obtain the electric field results.

The results are shown in Fig. 3.12 and Fig. 3.11, where it can be seen an zoomed image of the distribution of patches for a 0º tilt and 5º tilt respectively. It can be noticed that in order to recreate a 0º tilt all the patches must have the same width, therefore, the whole distribution will be made of equal patches.

(a) Upper platform   (b) 0º patches distribution
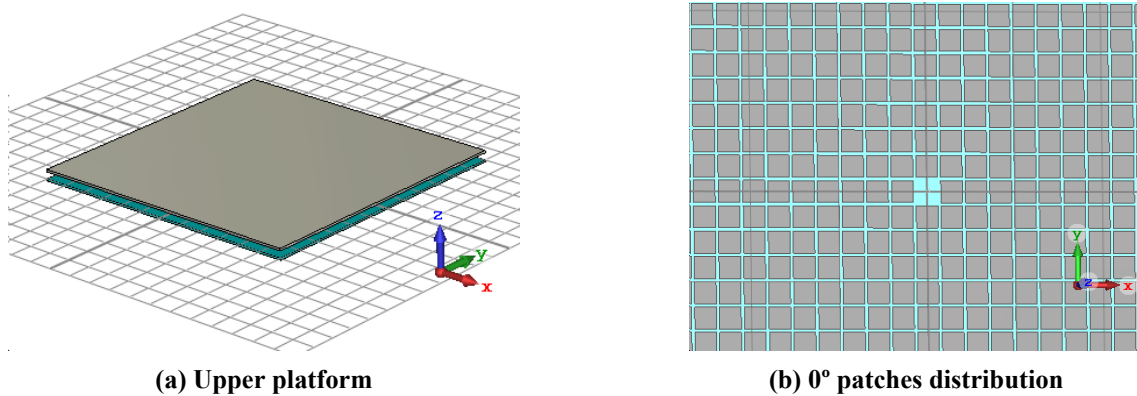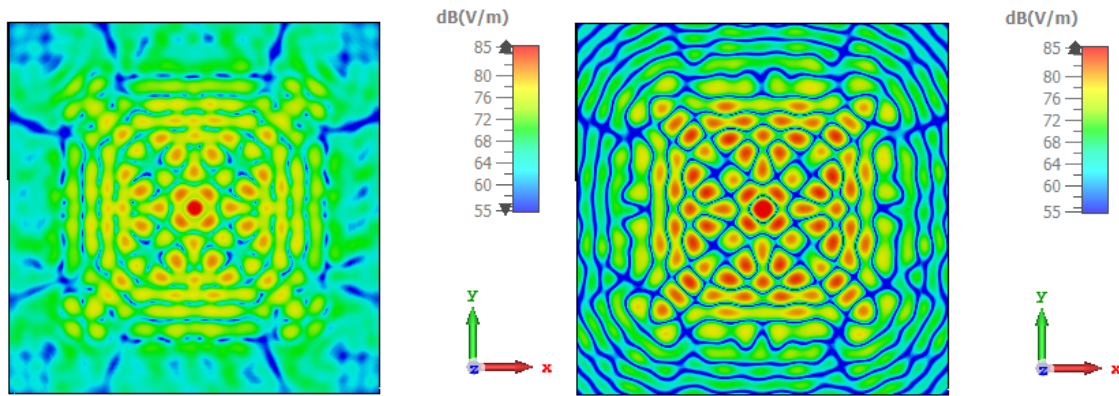
Figure 3.10: RLSA antenna without slots

Notwithstanding, as shown in Table 3.4 and previous studies, in order to get higher values of permittivity slotted-mushrooms are needed. For example, in Fig. 3.11 the distribution corresponds to a tilt of 5º.

(a) Upper-platform

(b) Metasurface using Patches and Slotted-Mushrooms
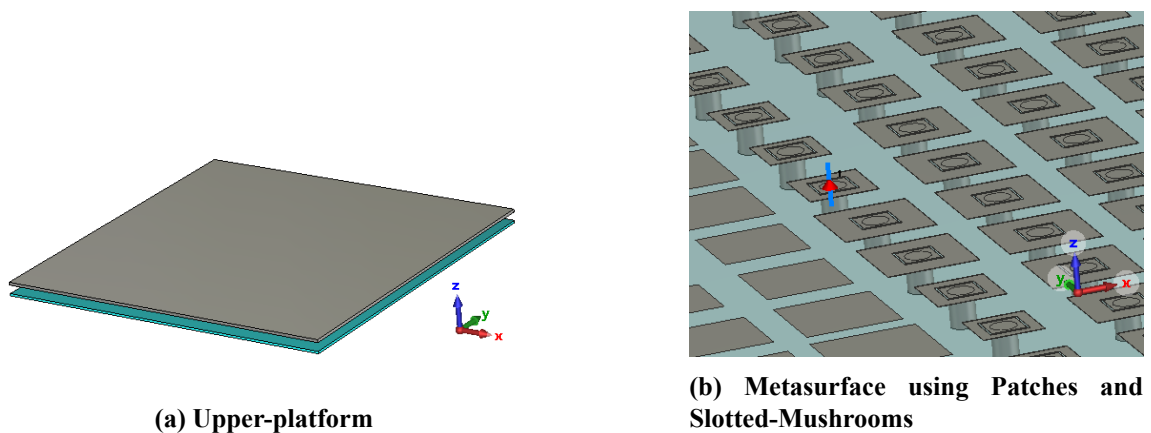
Figure 3.11: RLSA antenna without slots 5º tilt

Figure 3.12: Amplitude Electric field RLSA antenna, mesh = 5 tetrahedrons per wavelength, 0º tilt

Fig. 3.12 shows the result for a first analysis considering a distribution of patches with the same width and a mesh of 5 tetrahedrons per wavelength. The results are very unsatisfactory since no cylindrical distribution of the electric field is obtained. Therefore, in order to observe better its behavior, the mesh will be increased to 9 tetrahedrons per wavelength. The results for this mesh are those of Fig. 3.13.
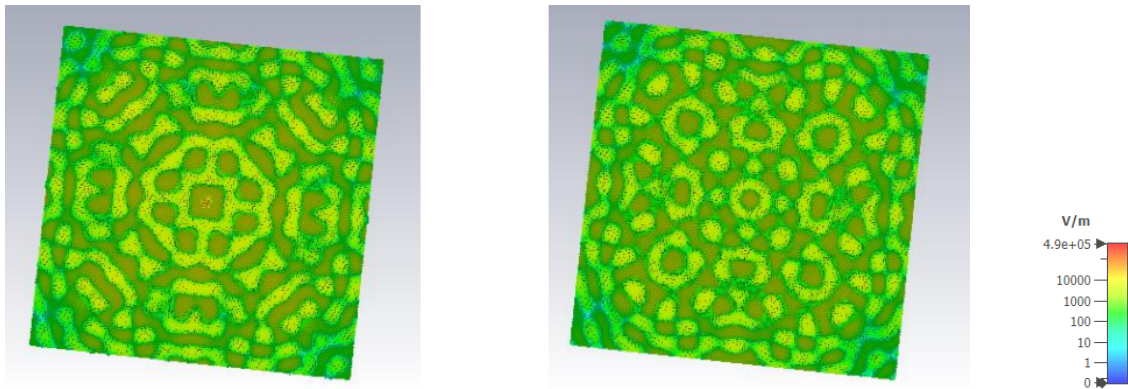
Figure 3.13: Electric field RLSA antenna, mesh = 9 tetrahedrons per wavelength, 0º tilt

The square shape of the patches forces the radial field to have this pattern, which can best be seen in Fig. 3.14. where Fig. 3.14a shows the electric field pattern obtained against electric field propagation that was obtained in [15] considering pin structures, Fig. 3.14b, where a radial propagation of the electric field is clearly observed.
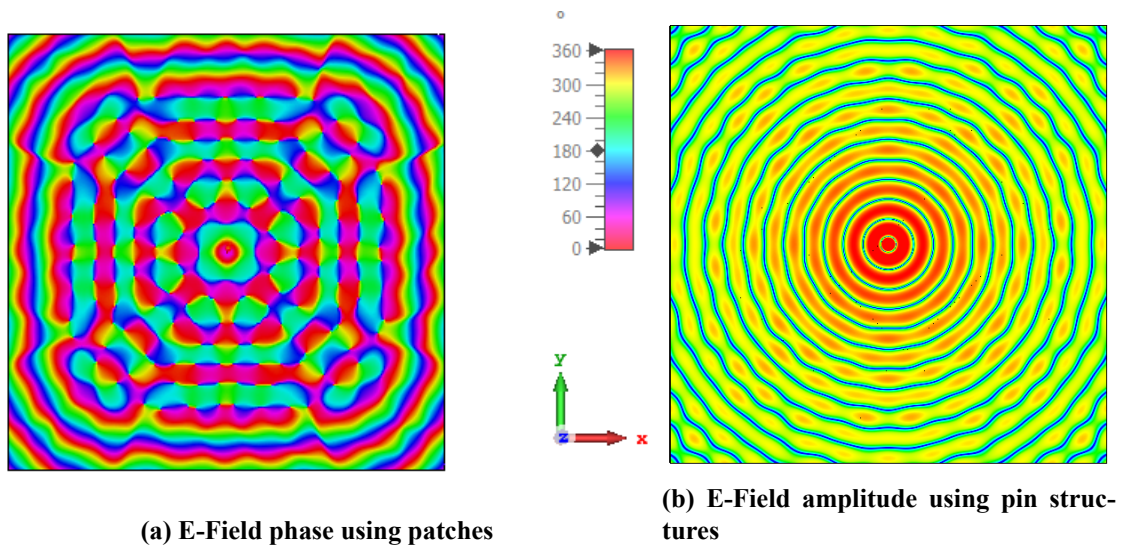
(a) E-Field phase using patches

(b) E-Field amplitude using pin structures

Figure 3.14: RLSA E-Field phase

The distribution of the elements found in Table 3.4 when considering a tilt value different than 0º, for instance 5º can be seen in Fig. 3.11

Therefore, the possibility of considering patches of a smaller size or another type of structure such as circular patches, rotated square patches or even hexagons was studied since these are more feasible. But, due to the simplicity of the patches and the cost of simulation time, it was considered the first option over the others. To reduce the size of the patches without the patches being too far apart from each other, as this could render them ineffective, the period size (cell width) must be reduced.

3.3.5   Second study: p = 1.5 mm and h_g = 3 mm

This study starts from the premise found during the first study in which it is shown that the patches must have a smaller width, and thus their period must be reduced in the same way. Therefore, the features considered will be a cell size of 1.5 mm and a waveguide height of 3 mm.

The study of the table of permittivities and patch sizes should be carried out again. The results obtained for this cell size are shown in Fig. 3.15, where it can be seen that the shape of the wavefront is much more cylindrical than in the previous study.

Distance between patches (mm)	β value	ε_{eff}	Patch width (mm)	Type of structure
0.1	1057	2.830	1.40	Slotted-Mushroom
0.11	1051	2.800	1.40	Slotted-Mushroom
0.12	1031	2.690	1.40	Slotted-Mushroom
0.13	1007	2.570	1.40	Slotted-Mushroom
0.1	996	2.513	1.40	Patch
0.12	980	2.433	1.38	Patch
0.15	952	2.296	1.35	Patch
0.2	921	2.150	1.30	Patch
0.25	882	1.971	1.25	Patch
0.3	858	1.865	1.20	Patch
0.35	831	1.749	1.15	Patch
0.4	810	1.662	1.10	Patch
0.5	780	1.541	1.00	Patch
0.6	759	1.459	0.90	Patch
0.7	743	1.398	0.80	Patch
0.8	731	1.354	0.70	Patch
1	721	1.317	0.50	Patch
1.1	717	1.302	0.40	Patch

Tabla 3.5: Patch width values depending on permittivity
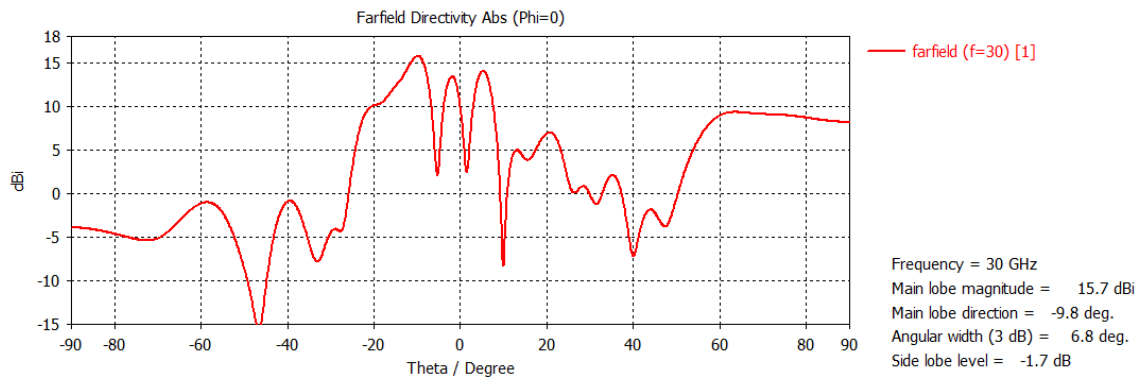

Figure 3.15: E-Field Phase 0º tilt

After observing that the electric field is already propagating radially, the far field radiation pattern must now be analyzed to see if the antenna reaches the required objectives.
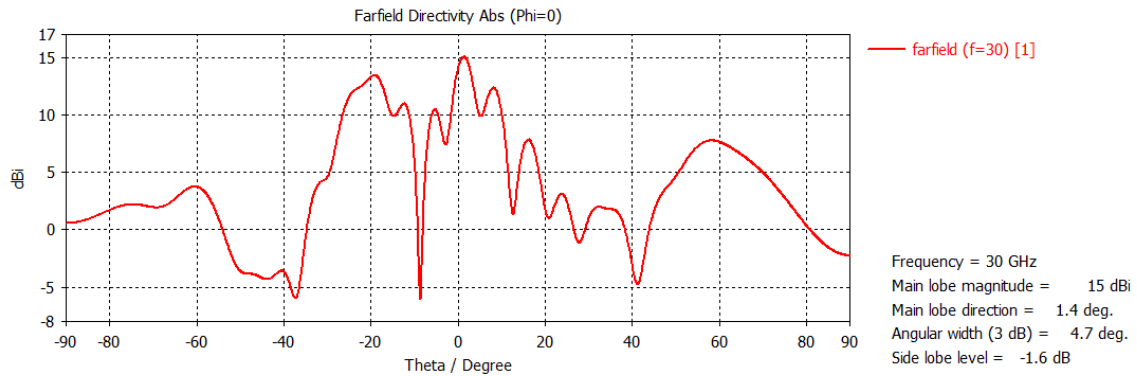

Figure 3.16: 5º tilt


Figure 3.17: 10º tilt

As can be seen in Fig. 3.16 and Fig. 3.17, the radiation patterns have secondary lobes at considerable high levels, as well as low directivity. Moreover, there is not a clear main lobe in the pattern. Thus, the results are not satisfactory and a further study of the structure must be carried out in order to determine where the problem can be.

Finally, after having investigated the reason for these patterns, it was concluded that the fundamental mode was mixing with mode 3 as was already explained in Fig. 3.3, this mode is more intense than the first one in the air zone, that is, the waveguide. As the tilt value is increased, the size of the patches gets larger according to Table 3.5 and therefore higher order modes appear.
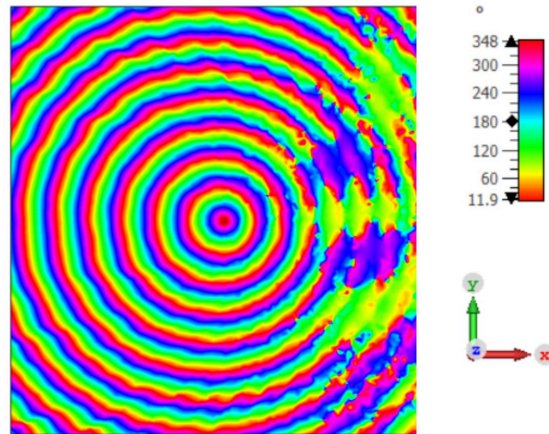
Figure 3.18: Mixing modes representation

Thus, a solution to this type of problem is to reduce the height of the waveguide so that only the fundamental mode can propagate through it. This waveguide height is reduced to 1 mm, $h_g = 1$ mm, and the study is performed again.
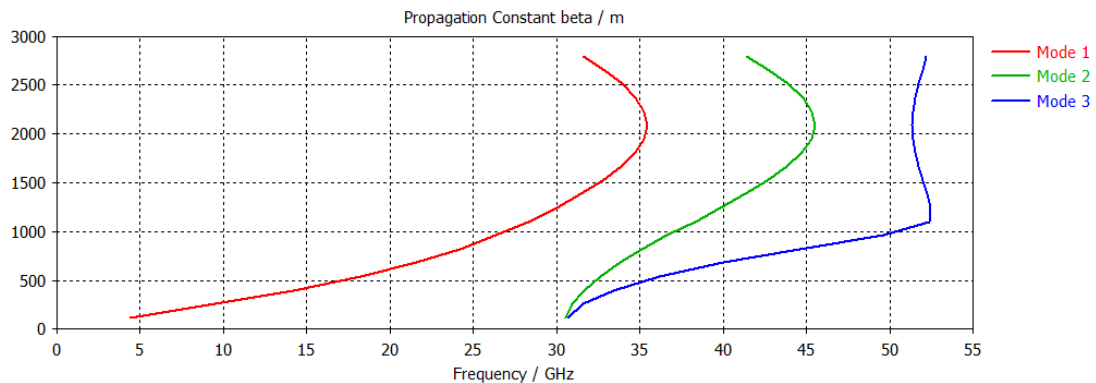
Figure 3.19: 10° tilt

3.3.6   Third study: p = 1.5 mm and h_g = 1 mm

In this section, the final metasurface structure will be introduced. This structure will be entirely made of patches as slotted-mushrooms don't offer good results, for example in Table 3.5 the interval of permittivity that can be reached thanks to slotted-mushrooms is not that significant, $\varepsilon_r = (2.57, 2.83)$ for this type of structure. So, as the simulation times are higher using mushrooms, and the fact that they don't give a large interval of permittivity, slotted-mushrooms will not be considered in future analysis.

In order to implement the metasurface, a table of values if permittivity is needed, as explained in previous sections. The information extracted from this table is shown in Table 3.6.

Distance between patches (mm)	β value	ε_{eff}	Patch width (mm)
0.1	1024.77	2.66	1.40
0.13	1001.6	2.54	1.37
0.15	988.6	2.48	1.35
0.2	961	2.34	1.30
0.25	938	2.23	1.25
0.3	918.7	2.14	1.20
0.4	885.6	1.99	1.10
0.5	862	1.88	1.00
0.6	843.6	1.80	1.00
0.7	831	1.75	0.90
0.8	822	1.71	0.80
0.9	815	1.68	0.70
1	810.9	1.67	0.50
1.1	807	1.65	0.40
1.2	806	1.645	0.30
1.3	804.8	1.64	0.20

Tabla 3.6: Patch width depending on permittivity value

In the first place, the distribution of patches and slots is studied for the case of a 5º tilt, this representation of such can be observed in Fig. 3.20a.
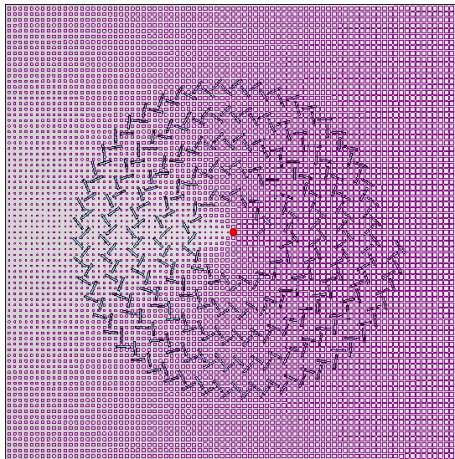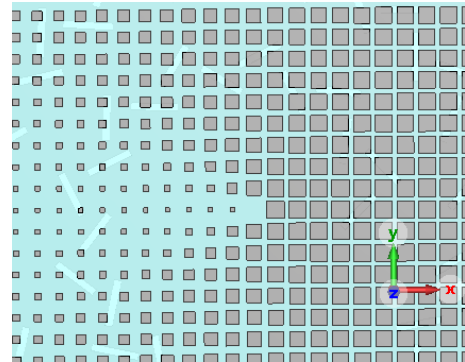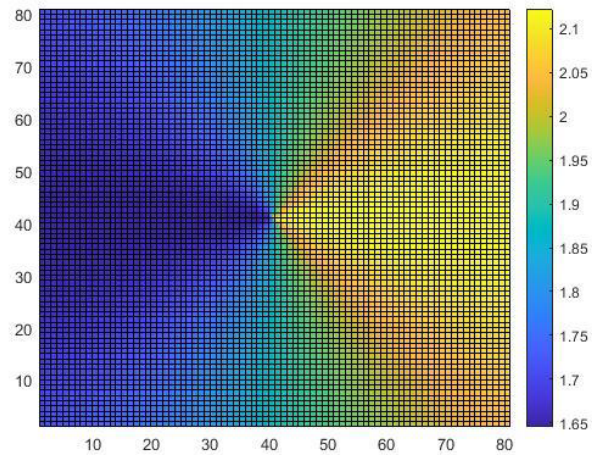

(a) Slots and patches distribution   (b) Metasurface using patches

Figure 3.20: RLSA 5º tilt

Figure 3.21: Permittivity interval in Matlab 5º tilt

As can be seen in Fig. 3.21, the interval of permittivity reached in Matlab in order to get a 5º tilt is approximately $\varepsilon_r = (1.65, 2.1)$. This interval can be found in Table 3.6, so it is possible to implement a metasurface in order to get a 5º tilt only using patches.

The phase is represented in Fig. 3.22
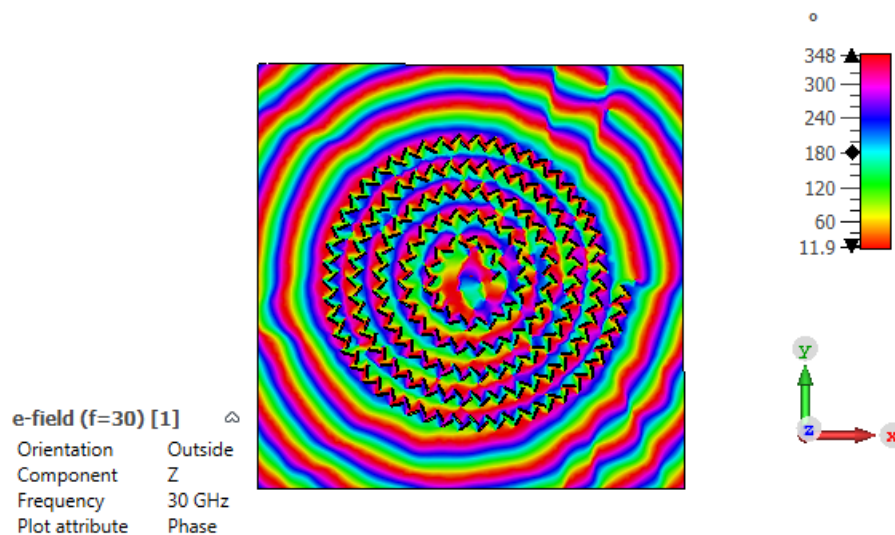
Figure 3.22: E-Field phase 5º tilt

The results obtained are satisfactory and can be seen in Fig. 3.23. The radiation pattern will be studied later in the final results section.
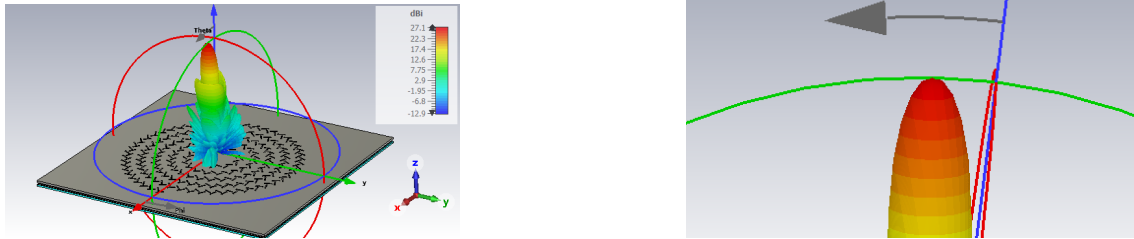
Figure 3.23: 5º tilt 3D pattern using CST

An analysis is carried out for the broadside case to corroborate the performance of the antenna. In this case, all patches take the same width value.
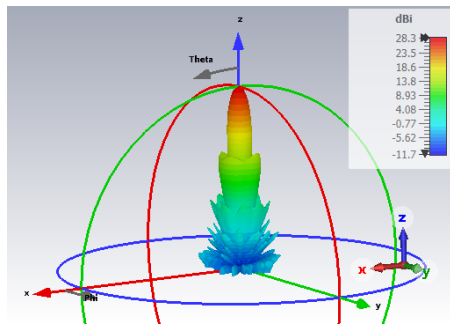
Figure 3.24: Broadside antenna 3D pattern using CST

As can be seen in Fig. 3.24, the pointing has a 0º inclination and the pattern looks fully directive.

Finally, the maximum tilt of the antenna must be found. Therefore, a tilt of 10º will be considered, for this structure the interval of permitivity values can be adjusted so that no mushrooms are needed, but smaller patches. For convenience, only patches will be used. The result can be seen in Fig. 3.25, where a very high level of secondary lobes and low directivity can be seen. Therefore, the limit tilt will have a value lower than 10º.

Figure 3.25: 10º tilt cartesian pattern

So far, the results show that the maximum angle will be a number between 5º and 10º tilt. Now,

an angle of 7.5° will be considered. The results are shown in Fig. 3.26.
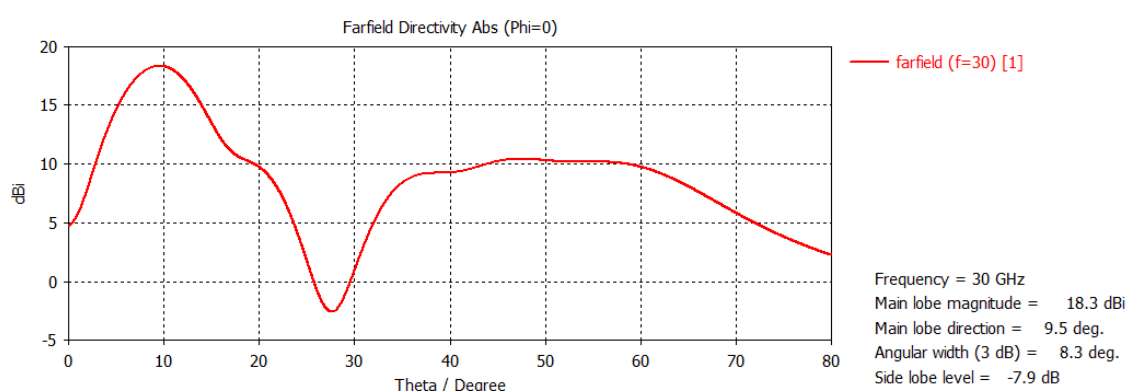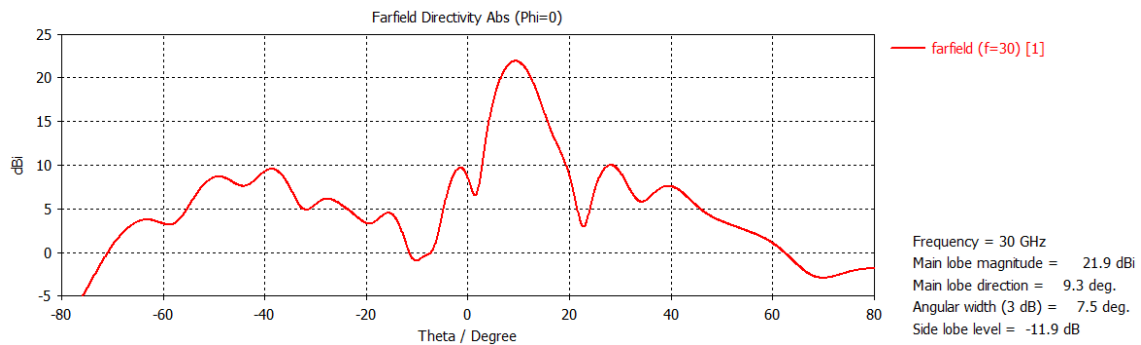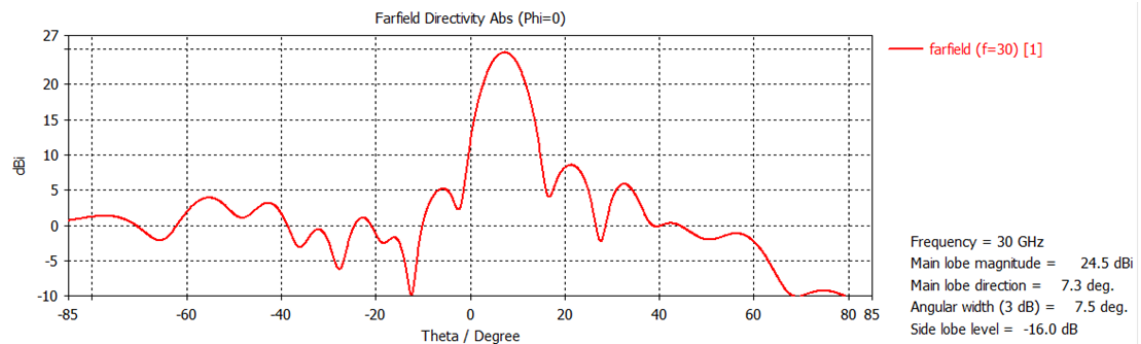

Figure 3.26: 7.5° tilt cartesian pattern

As can be seen in Fig. 3.26, the main lobe direction is 9.3° when it should be value around 7.5°, moreover, there can be seen high values of secondary side lobes level. Thus, another study for an angle between 5° and 7.5 must be carried out. The following angle considered is 6°.

Figure 3.27: 6° tilt cartesian pattern

As the limit angle approaches a value of 5°, the radiation pattern results are improved, but in the case of a 6° tilt angle as shown in Fig. 3.27 even though the pattern seems to present good SLL values and directivity, the main lobe direction presents and angle of 7.3° when it should be a value around 6°.

Thus, the maximum tilt value is 5° for this antenna. Notwithstanding, this angle can be increased by changing the arrangement of the different parts of the antenna. The analysis of the results and all the necessary changes in order to get higher tilt values will be explained during the following chapter.

Chapter 4

Final results

In this chapter, final results obtained through CST for a metasurface design consisting of patches will be introduced. The models that will be presented below refer to different values of beam-steering, which will also show other parameters of interest such as angular width or SLL level.

The process of construction and modeling of the antenna layout in CST starts from the following steps: first, the bed of patches is imported, those patches are created as thin layers with zero thickness to relax computational cost. Just below this bed of patches is placed the 0.787 mm thick dielectric substrate according to the standard dielectric thickness sizes. Finally, the platform is created where the imported slots generated in Matlab are embedded. This platform is 1 mm thick and is located at a height of h_g = 1 mm from the metasurface.

Finally, the boundary conditions are established, as well as the field and port position monitors, and then the simulation is performed using the Frequency Domain Solver. In Fig. 4.1 an example of a complete antenna can be seen prior to its simulation. Table 4.1 compiles all the design parameters that the antennas hold in common, which will be analyzed in further sections.

- ε_r: Relative permittivity of the dielectric.

- **N**: Number of slot turns in the upper platform.

- t_{res}: percentage of residual power transmitted.

- w_r: Slot width.

- th_r: Slot thickness.

Parameter	f_0 (GHz)	ε_r	N	t_{res}	d (mm)	w_r (mm)	th_r (mm)
Value	30	4	5	0.9	1	0.5	1

Tabla 4.1: CP-RLSA Design parameters

In order to generate the slots, the value of the parameter S_ρ applied for the implementation of the metasurface is used, from which the relative permittivity is extracted following the relationship established in (4.1).

$$\varepsilon_r = \left(\frac{1}{S_\rho}\right)^2 \tag{4.1}$$

4.1 Beam-steering methods

To obtain different tilt values, several methods can be carried out. In the first place, it should be noted that the antenna is made up of two plates which also form the waveguide, one containing the patches and the other the slots in it. In order to form the beam-steering, there exists two different methods:

- **Method 1**: Slots distribution for an angle of 0º and 5º tilt patches distribution (Fig. 4.1).

- **Method 2**: Slots distribution for an angle of $\theta = 5°$ and uniform patches distribution (broadside) (Fig. 4.2).

In Fig. 4.1a the slot distribution in the upper plate is equispaced in other to offer a broadside transmission of the field whilst on the lower plate the distribution of patches offers a beam-steering of 5º. In this case, the lower plate is the one that determines the tilt angle, while the slots distribution does not modify the field propagation.

In Fig. 4.1b the patches present a uniform distribution offering a broadside propagation of the electric field, and the upper plate containing the slots determine the tilt value, that is the beam-steering. As can be seen the turns of the slots are rearranged in a way that every turn is closer to one another in the left part while they are more distant in the right one. With this new arrangement of the turns of slots, the beam-steering is formed at a specific angle, which in this case is 5º.

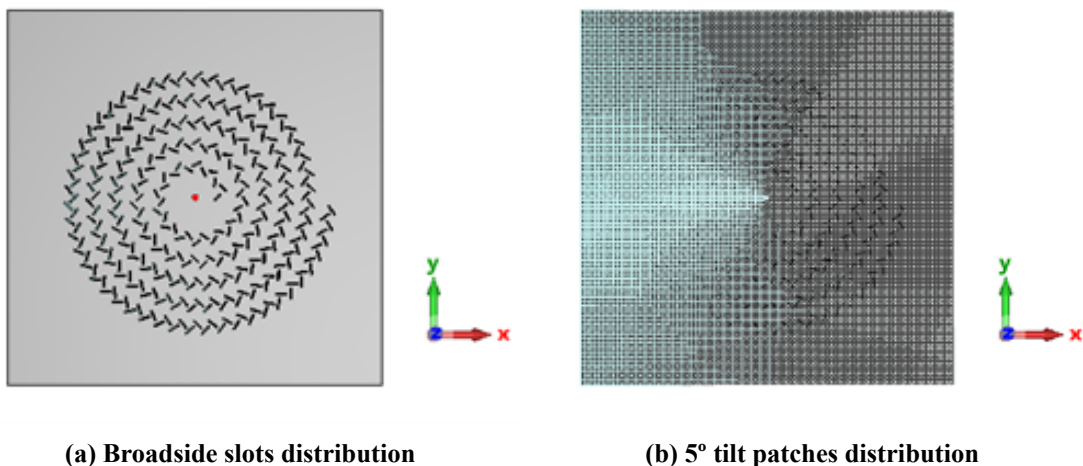(a) Broadside slots distribution   (b) 5º tilt patches distribution

Figure 4.1: Method 1

(a) 5º tilt slots distribution   **(b) Broadside distribution of patches**
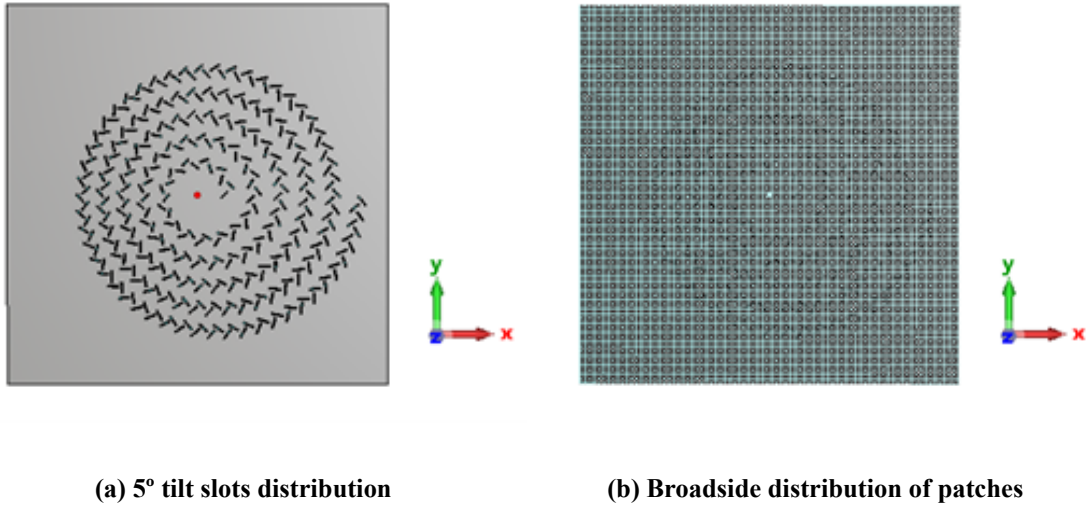
Figure 4.2: Method 2

Furthermore, it is possible to achieve higher tilt values by combining the structures in Fig. 4.1 and Fig. 4.2. Although, Method 1 will be the one considered in order to get the chosen value of tilt, this idea will also be studied during the following sections.

4.2   Broadside antenna

In the first place, a broadside type antenna will be considered. This term comes from the fact that the slots used are endowed with a null beam steering, so the maximum of the radiation pattern will be in the broadside direction $\theta = 0º$, that is, perpendicular to the structure.

In Fig. 4.3, the structure and design of an antenna of these characteristics is shown. Unlike Figs. 4.1 and 4.2, there is no need to either implement a specific patches or slots distribution to get a broadside propagation of the electric field. In this case, the turns of the slots in the upper plate as well as the distribution of patches will be uniform.

As can be seen, a model of N = 5 turns of slots has been used. The relative permittivity value will be $\varepsilon_r = 1.7778$ according to (4.1).
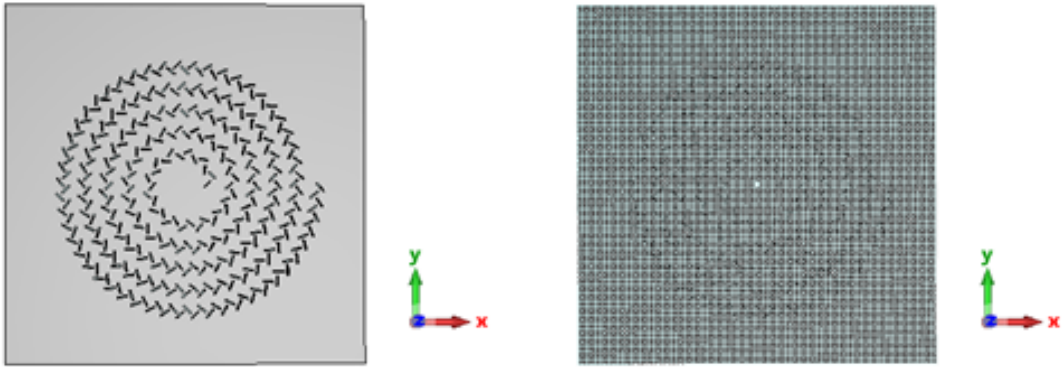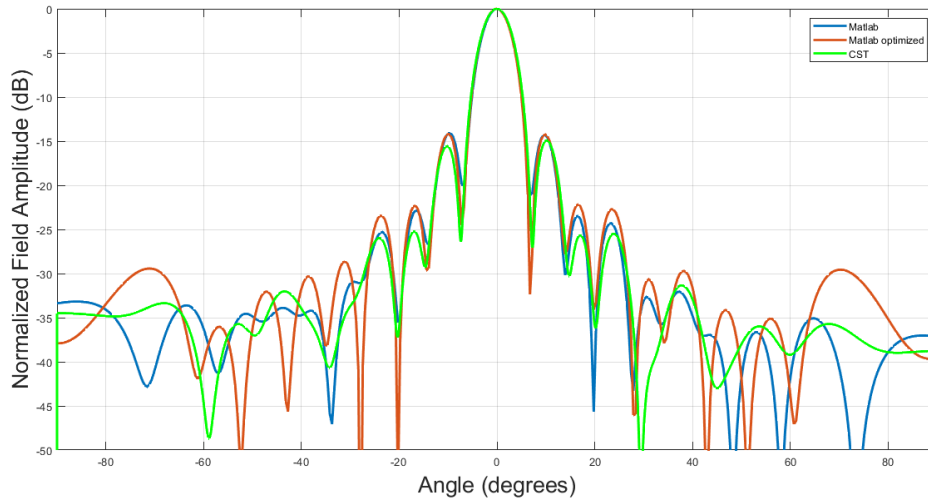
Figure 4.3: CP-RLSA broadside antenna

Figure 4.4: Comparison of radiation patterns: CST vs Matlab broadside distribution

The operating parameters of this antenna are listed in Table 4.2.

Parameter	$D_{\mathbf{max}}$ (dBi)	SLL (dB)	$\nabla\theta_{-3dB}$ (°)
Value	28.3	-14.9	6.3

Tabla 4.2: Broadside CP-RLSA antenna parameters

In Fig. 4.4 radiation patterns shown belong to the results obtained using Matlab and CST software after simulating the whole structure.

As regards Matlab distribution, there can be seen that the secondary lobes are more defined and higher than the ones shown in the CST distribution, there is also a slightly difference between the nulls depths. This latter issue happens because of the fact that in Matlab the cross-polar component of the field is not taken into account, whilst in CST that component is indeed considered.

4.3 5º tilt antenna

As regards antennas with a 5º tilt, the metasurface will no longer be uniform and will have an azimuthal distribution of patches as shown in Fig. 4.5. Likewise, the distribution of slots will maintain a tilt of 0º, however the relative permittivity will be different altering the distribution of slots. That is, in order to get a central distribution of patches as shown in Fig. 3.9, the parameter S_ρ needs to be changed, and attending (4.1), the value of the relative permittivity ε_r will change as well. Therefore, ε_r needs to be changed in the Matlab code that implements the distribution of slots. The permittivity for this case will be $\varepsilon_r = 1.8765$.

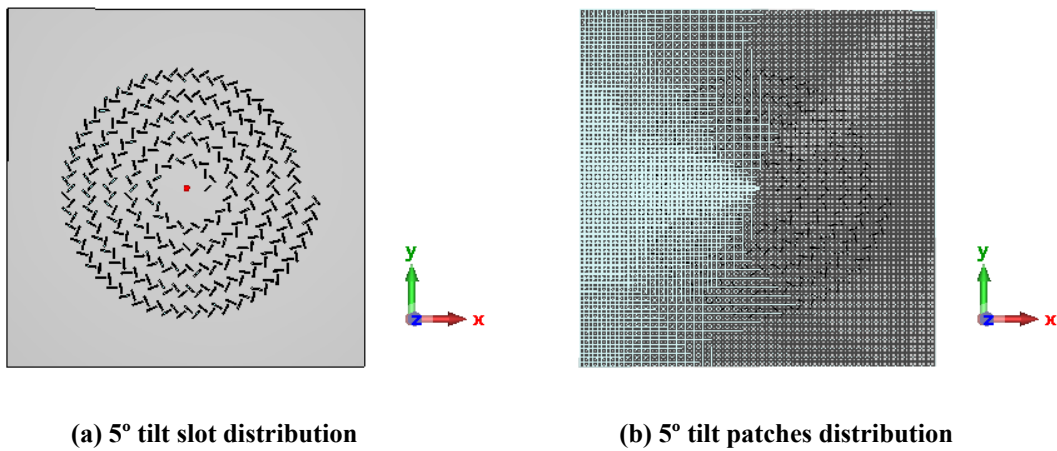(a) 5º tilt slot distribution   (b) 5º tilt patches distribution

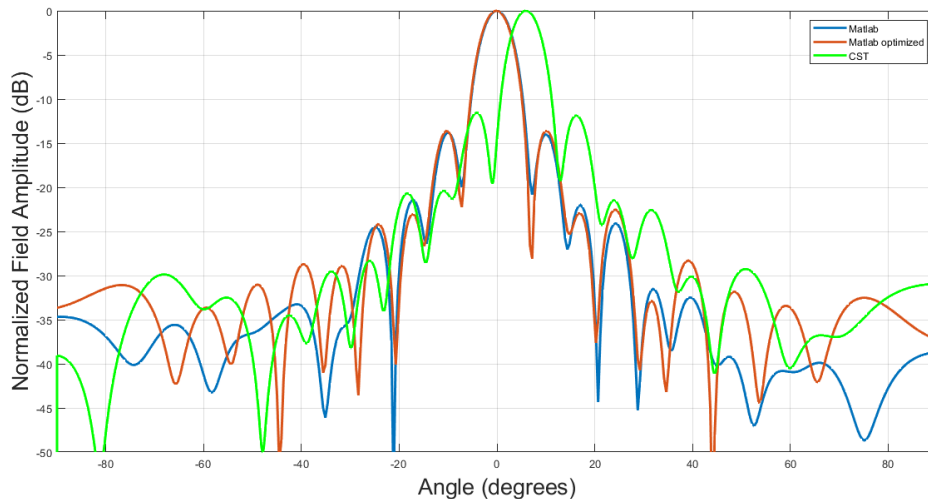**Figure 4.5: CP-RLSA 5º tilt antenna**

Figure 4.6: Comparison of radiation patterns: CST vs Matlab 5º tilt distribution

In Fig. 4.6, it can be seen that the distribution of patches on the metasurface causes the beam

steering of 5º, since the curves obtained in Matlab refer to the radiation pattern provided by the slots only.

In this case, secondary lobes reach higher values in CST, and seem to be more stable and similar between them up to $\theta = |40º|$. Furthermore, the differences between both software are associated to the fact that, as explained during the last section, in CST the cross-polar component of polarization is considered, which is higher for angles where there is huge differences between both diagrams.

Parameter	D_{max} (dBi)	SSL (dB)	$\nabla\theta_{-3dB}$ (º)
Value	27.1	-11.6	6.2

Tabla 4.3: Broadside CP-RLSA antenna parameters

On the other hand, a configuration very similar to Fig. 4.2 could also be considered in order to get a 5º beam steering, where the slots provoke the inclination of the beam. The results of this configuration can be seen in Fig. 4.7.

(a) 5º tilt slot distribution   (b) 5º tilt patches distribution
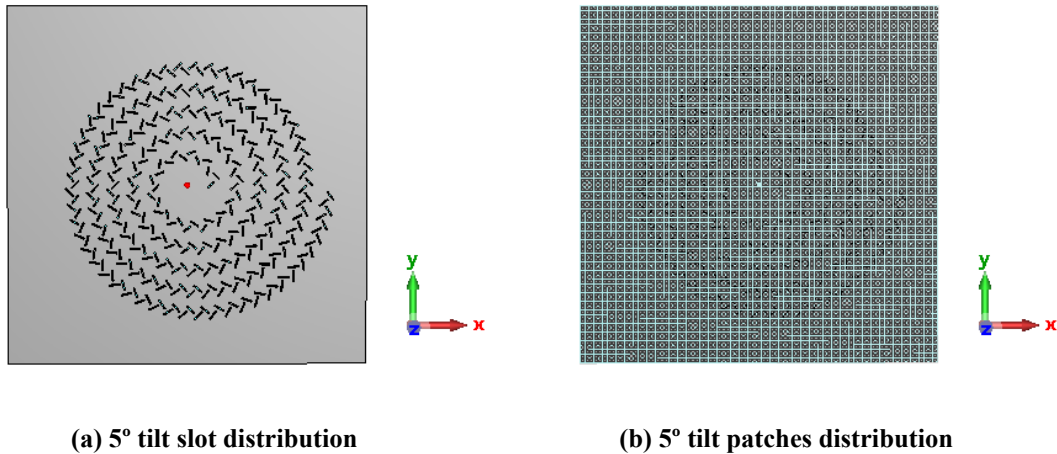
Figure 4.7: CP-RLSA 5º tilt antenna

Parameter	D_{max} (dBi)	SSL (dB)	$\nabla\theta_{-3dB}$ (º)
Value	28.2	-15	6.3

Tabla 4.4: Broadside CP-RLSA antenna parameters
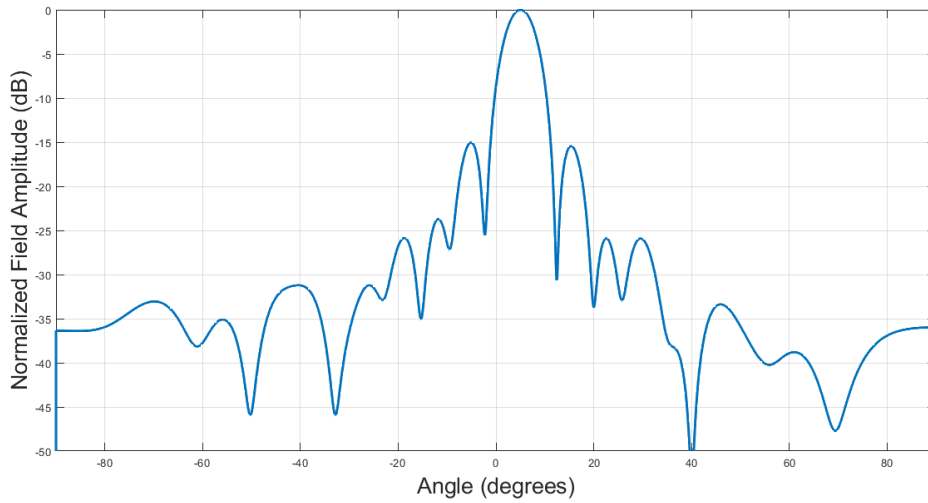
Figure 4.8: Radiation pattern in Matlab 5º tilt distribution

4.4   Antennas with rotating upper plate

In this section, a study of different combinations of metasurface distribution and slots will be carried out in order to achieve higher tilt values than those seen during the previous sections. Moreover, the rotation of the upper plate will be introduced to redirect the pointing of the antenna at different angles not achievable by the antenna itself. The rotation of the plate will be based on the fundamentals of the Risley prism theory defined in [21] where an antenna with the same characteristics is shown and the theoretical model seen in chapter 2. Specifically, in the following subsections a study of the effects of rotating the upper plate of the waveguide will be specified making use of the combination of the models described in figures 4.1 and 4.2, with which it will be possible to increase the limit angle and shape it just by rotating the upper plate around the z axis through an angle of 180º and 90º.

4.4.1   0º rotation

In this study, the slots will be spread out around the upper plate considering a 5º distribution, and as for the patches distribution, a 5º tilt distribution will be considered as shown in Fig. 4.9. The result, as demonstrated above, should offer a beam-steering angle twice the one each platform can propagate.
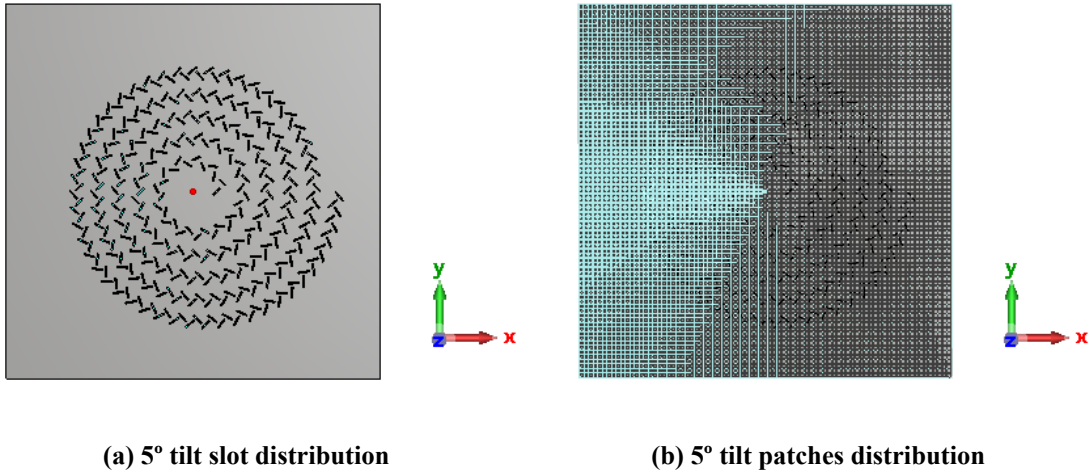
(a) 5º tilt slot distribution   (b) 5º tilt patches distribution

Figure 4.9: CP-RLSA 5º tilt antenna

In Fig. 4.10 it can be seen that the beam-steering angle is $\theta = 10.8$, therefore, it can be stated that the antenna meets the expectations proposed for this tilt value as studied in (2.15). Furthermore, SSL and directivity values are optimum and the beam width is not high, notwithstanding there can be observed a gratin lobe in the left side of the diagram.
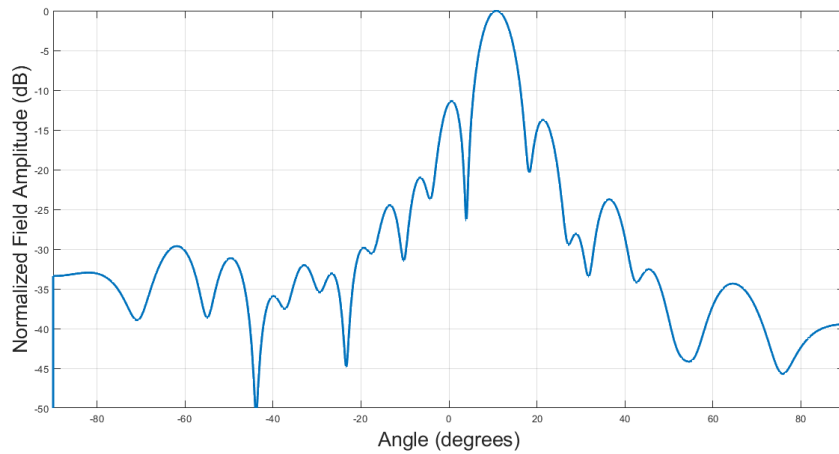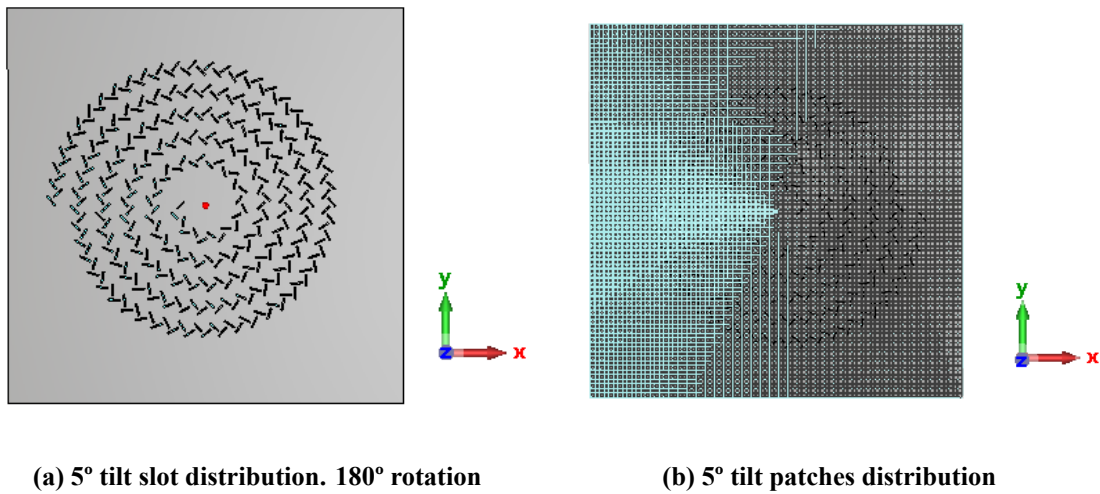

Figure 4.10: Radiation pattern for a CP-RLSA antenna with a 5º tilt distribution of slots and patches in CST

Parameter	$D_{\mathbf{max}}$ (dBi)	SSL (dB)	$\nabla\theta_{-3dB}$ (º)
Value	27.5	-11.4	6.3

Tabla 4.5: Double 5º tilt CP-RLSA antenna parameters

4.4.2 180º rotation

As has been demonstrated in (2.17), if the platform of the slots is rotated 180º with respect to that of the patches, the effects of both are counteracted and, therefore, a broadside case should be obtained. In Fig. 4.11, the design of the antenna under these characteristics can be seen, where the upper plate has been rotated 180 degrees while the lower one has the same patch distribution as in Fig. 4.9b.

(a) 5º tilt slot distribution. 180º rotation   (b) 5º tilt patches distribution

Figure 4.11: CP-RLSA 5º tilt antenna. Upper platform rotated 180º

The radiation pattern obtained in this design is shown in Fig. 4.12, where it can be seen that the pointing angle is practically 0 degrees.
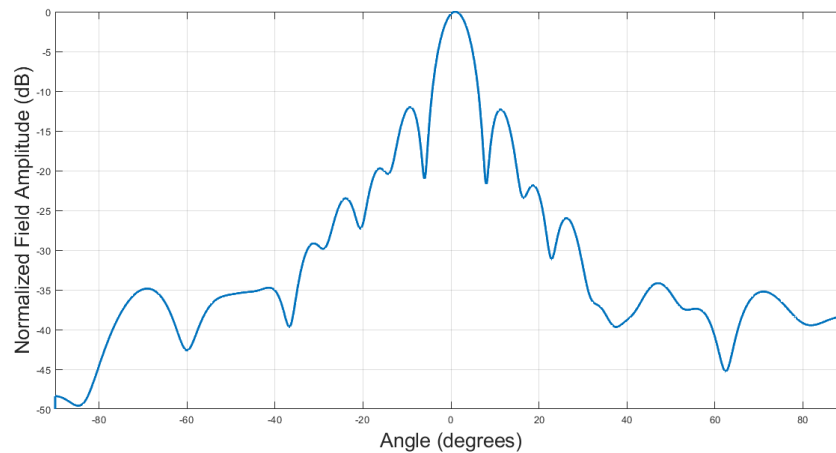
Figure 4.12: Radiation pattern for a CP-RLSA antenna with a 5º tilt distribution of slots and patches in CST and the upper plate rotated 180º

| Parameter	D_{max} (dBi)	SSL (dB)	$\nabla\theta_{-3dB}$ (°)
Value	27.5	-12	6.2

Tabla 4.6: 5º tilt CP-RLSA antenna parameters. Upper plate rotated 180º

4.4.3   90º rotation

In this case, the upper plate will be rotated 90º to verify the third case in which an angle of tilt of 5º was considered. The arrangement of the platforms can be seen in Fig. 4.13 where it can be observed that again the distribution of patches is the same.
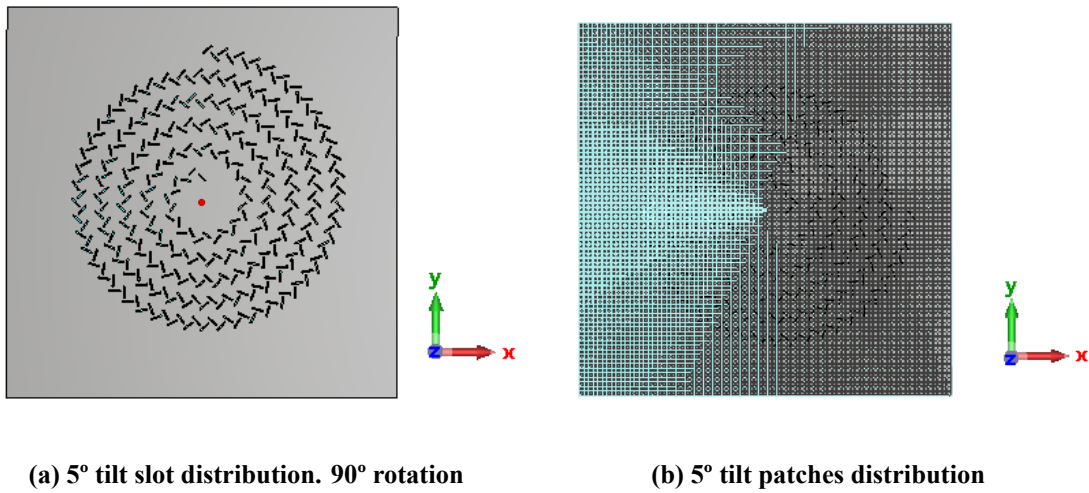
(a) 5º tilt slot distribution. 90º rotation   (b) 5º tilt patches distribution

Figure 4.13: CP-RLSA 5º tilt antenna. Upper platform rotated 90º

The beam-steering angle for this case should adopt an intermediate value between the case of 180º, where a result of 10º was obtained, and the broadside case, that is, around 5º. Conversely, in this case as the platform is rotated 90º, the beam will also rotate in the azimuth direction. The maximum will take place at a cut of $\phi = 45$.

As can be seen in Fig. 4.14, the design meets the premises.

Parameter	D_{max} (dBi)	SLL (dB)	$\nabla\theta_{-3dB}$ (°)
Value	27.6	-13.1	6.4

Tabla 4.7: 5º tilt CP-RLSA antenna parameters. Upper plate rotated 90º
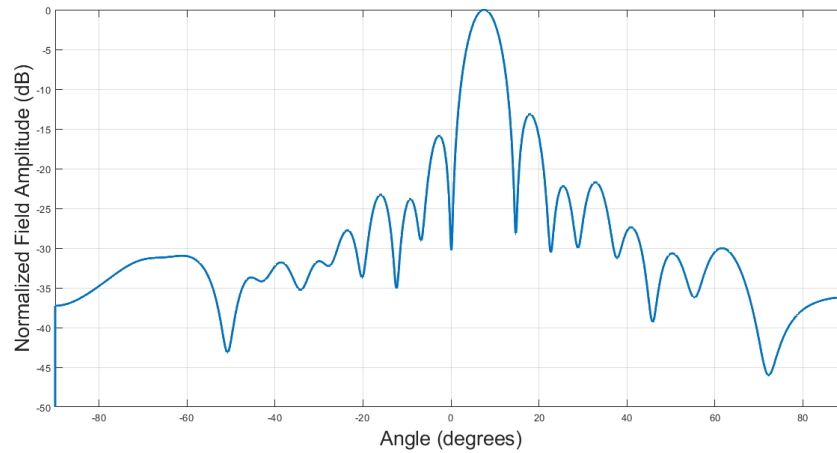
Figure 4.14: Radiation pattern for a CP-RLSA antenna with a 5º tilt distribution of slots and patches in CST and the upper plate rotated 90º

After having analyzed three ways to change the beam-steering of the antenna by means of spinning the upper platform, the results of such are shown in Table 4.8, where it can be seen that the values of directivity, SLL and beam width are quite similar. It can be concluded that the antenna offer good results and it is easy to modify any characteristic of such just by adjusting physical changes on it.

Antenna	$D_{\mathbf{max}}$ (dBi)	SSL (dB)	$\nabla\theta_{-3dB}$ (º)
0º rotation	27.5	-11.4	6.3
180º rotation	27.5	-12	6.2
90º rotation	27.6	-13.1	6.4

Tabla 4.8: Comparison table
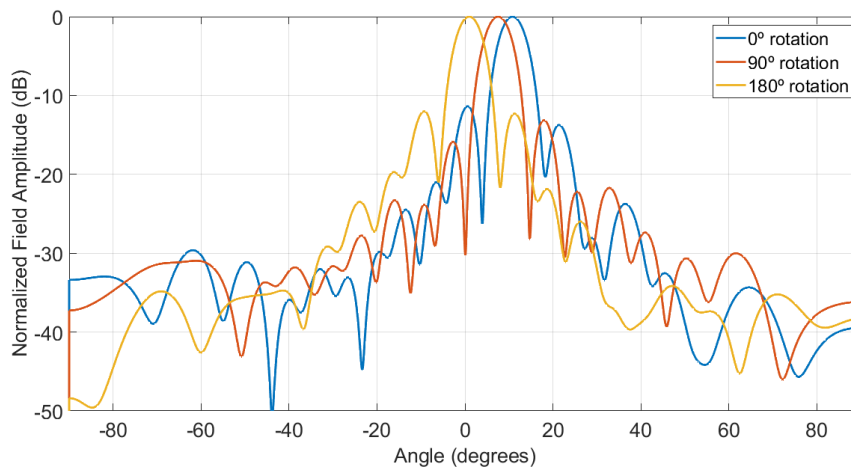
Figure 4.15: Comparison diagram

Chapter 5

Conclusions

After having disclosed the final results for this antenna which operates at 30 GHz, a final analysis and evaluation of the antenna can be carried out. In general, the concept of using an antenna of this type is a great advantage in different sectors such as satellite communications, which we have focused on during this project. It is especially useful in applications which require high gain and Low Profile antennas. In addition, due to the fact that the metamaterial is simply a printed circuit board, the manufacturing will be low cost. Regarding the antenna studied during this project, in the first place, it should be noted that the fact of having analyzed three types of structures for the implementation of the metasurface, and especially due to the introduction of mushrooms, has made it difficult to find a range of permittivities. The mushrooms have not turned out to give the expected results, instead they offered longer simulation times and made it difficult for the electric field to propagate radially. Although, it should also be noted that, since it is a periodic surface, once the structure of the cell unit has been obtained, its implementation is relatively simple, and this has caused passive electromagnetic devices to have opted for integrating this type of EBG metasurface. Regarding the generation of slots, the process has been facilitated by the use of Matlab codes generated in [10]. These codes were provided from the beginning of the project and have been of great help, especially because in this way a simulator has not been needed that could have complicated and multiplied the simulation times of the antenna.

After having analyzed the final results obtained in a global way, it can be concluded that the antenna construction process has been laborious, taking into account the previously exposed limitations. In a first case, if a metasurface is considered with all the patches of the same size, that is to say, broadside distribution, it is true that configuring the rings of the upper plate for different angles causes the beam steering to point at the angle established by this plate. However, when a broadside centralized distribution of the slots in the upper plate is considered, in such a way that the radial distribution of patches of different sizes above the dielectric of the lower plate is what causes the beam steering, there exists a limit angle at 5º. This is a very low tilt value, so the chosen metasurface made up of variant patches size does not perform as well as the pins in [15]. Furthermore, the fact of having reduced the size of the cells makes this antenna difficult to make due to its size, it is not possible to build patches of such a small size, since some of them measure around 1 mm.

GLOSSARY

SATCOM   Satellite Comunications

SOTM   Satellite On The Move

AWGN   Additive White Gaussian Noise

EIRP   Effective Isotropic Radiated Power

RLSA   Radial Linear Slot Antenna

CP-RLSA   Circular Polarized Radial Linear Slot Antenna

SL-RLSA   Single Layer Radial Linear Slot Antenna

EBG   Electromagntic Bandgap

TEM   Transverse Electric and Magnetic Field

PEC   Perfect Electric Conductor

SLL   Sidelobe Level

Bibliography

[1] klaus krippendorff klaus. "Mathematical Theory of Communication". In: *Departmental Papers (ASC)* (Jan. 1964).

[2] A.J. Paulraj, R.U. Nabar, and D.A. Gore. "Introduction to Space-Time Wireless Communications [M]". In: (Jan. 2003).

[3] Ergin Dinc et al. "In-Flight Broadband Connectivity: Architectures and Business Models for High Capacity Air-to-Ground Communications". In: *IEEE Communications Magazine* 1 (Aug. 2017). DOI: `10.1109/MCOM.2017.1601181`.

[4] Sergey Borisov and Alexander Shishlov. "Antennas for Satcom-on-the-Move, Review". In: *2014 International Conference on Engineering and Telecommunication*. 2014, pp. 3–7. DOI: `10.1109/EnT.2014.12`.

[5] Zanming LIANG. *DVAC-1 CONCEPT DESCRIPTION: OFFSET GREGORIAN DISH VERSION E*. URL: `https://www.skatelescope.org/public/2011-07-13_Dish_Array_CoDR/WP2-020.045.010-TD-002-E_Dishb-ogchina.pdf`.

[6] ThinKom. *Phased array antenna*. URL: `https://www.thinkom.com/land/mobile/`.

[7] Yunfei Sun et al. "A Beam-Steerable Lens Antenna for Ku-Band High-Power Microwave Applications". In: *IEEE Transactions on Antennas and Propagation* 68.11 (2020), pp. 7580–7583. DOI: `10.1109/TAP.2020.2979282`.

[8] CST Microwave Studio. *Release Version 2021.02 - Jan 06 2021*. Dassault Systemes Deutschland GmbH, 2020.

[9] MATLAB. *version 9.9.0.1524771 (R2020b)*. Natick, Massachusetts: The MathWorks Inc., 2020.

[10] J. I. Herranz Herruzo. *Análisis y optimización eficiente de agrupaciones de ranuras en guía*. PhD thesis, 2016.

[11] Teddy P Purnamirza. "Radial Line Slot Array (RLSA) Antennas". In: Oct. 2019. ISBN: 978-1-78984-293-7. DOI: `10.5772/intechopen.87164`.

[12] K. Kelly and F. Goebels. "Annular slot monopulse antenna arrays". In: *IEEE Transactions on Antennas and Propagation* 12.4 (1964), pp. 391–403. DOI: `10.1109/TAP.1964.1138263`.

[13] M. Ando et al. "A radial line slot antenna for 12 GHz satellite TV reception". In: *IEEE Transactions on Antennas and Propagation* 33 (1985), pp. 1347–1353.

[14] M. Ando et al. "A slot design for uniform aperture field distribution in single-layered radial line slot antennas". In: *International Symposium on Antennas and Propagation Society, Merging Technologies for the 90's* (1990), 930–933 vol.2.

[15]   K Ortuño Mula. *Antena de ranuras en guía radial con haz reorientable en banda Ka*. PhD thesis, 2020.

[16]   Nanfang Yu and Federico Capasso. "Optical Metasurfaces and Prospect of Their Applications Including Fiber Optics". In: *Journal of Lightwave Technology* 33.12 (2015), pp. 2344–2358. DOI: 10.1109/JLT.2015.2404860.

[17]   Jing Wen et al. "Plasmonic Holographic Metasurfaces for Generation of Vector Optical Beams". In: *IEEE Photonics Journal* 9.1 (2017), pp. 1–8. DOI: 10.1109/JPHOT.2017.2651981.

[18]   Gonzalo Expósito-Domínguez et al. "Revision of EBG metamaterials and active antennas". In: *2012 6th European Conference on Antennas and Propagation (EUCAP)*. 2012, pp. 1–4. DOI: 10.1109/EuCAP.2012.6206660.

[19]   Ashraf Uz Zaman et al. "Gap Waveguide PMC Packaging for Improved Isolation of Circuit Components in High-Frequency Microwave Modules". In: *IEEE Transactions on Components, Packaging and Manufacturing Technology* 4.1 (2014), pp. 16–25. DOI: 10.1109/TCPMT.2013.2271651.

[20]   Ming Huang et al. "A 2-D Multibeam Half Maxwell Fish-Eye Lens Antenna Using High Impedance Surfaces". In: *IEEE Antennas and Wireless Propagation Letters* 13 (2014), pp. 365–368. DOI: 10.1109/LAWP.2014.2306207.

[21]   Bradley J Tame and Nathan A Stutzke. "Steerable Risley Prism antennas with low side lobes in the Ka band". In: *2010 IEEE International Conference on Wireless Information Technology and Systems*. 2010, pp. 1–4. DOI: 10.1109/ICWITS.2010.5611931.